Specific cell states underlie complex tissue regeneration in spiny mice

Emilio Oviedo Rivadeneira[1], Robyn Allen[1], Mike Adam[2], and Ashley W. Seifert[1,3,4*]

[1]*Department of Biology, University of Kentucky, Lexington, KY 40506, USA*
[2]*Division of Experimental Hematology and Cancer Biology, Cancer and Blood Diseases Institute, Cincinnati Children's Hospital Medical Center, Cincinnati, OH, USA*
[3]*Department of Veterinary Anatomy and Physiology, University of Nairobi, Nairobi, Kenya*
[4]*Aligning Science Across Parkinson's (ASAP) Collaborative Research Network, Chevy Chase, MD 20815, USA*

ORCID: Ashley W. Seifert, 0000-0001-6576-3664

Key words: Cell proliferation, regeneration, cell cycle, cell state, fibroblasts, chondroblasts

*To whom correspondence should be addressed: Ashley W. Seifert, e-mail: awseifert@uky.edu

SUMMARY STATEMENT

Comparing regenerative vs. fibrotic healing, we identify injury-induced cell states associated with persistent cell cycle progression and complex tissue regeneration in mammals.

ABSTRACT

Cell proliferation is an elemental feature of epimorphic regeneration in vertebrate taxa. We previously reported that in contrast to fibrotic repair observed in laboratory mouse (*Mus*) strains, highly regenerative spiny mice (*Acomys* spp.) exhibit cell cycle progression and cell proliferation to faithfully replace missing tissue. However, little is known about proliferation dynamics, and specific cell types and states that may contribute to complex tissue regeneration in mammals. Using temporal pulse-chase experiments, we show that stromal cells in *Acomys dimidiatus* rapidly re-enter the cell cycle in response to injury and maintain tight spatiotemporal control of cell cycle progression to restrict the proliferative population to a distal area relative to the injury. Conversely, *Mus* stromal cells incorporate thymidine analogs without cell division supporting an S-phase arrest after D10. Deploying immunostaining and scRNA-seq, we identify several key cell types (CRABP1+, αSMA+) differentially associated with regenerating versus scar tissue. Importantly, our single cell data revealed distinct gene expression profiles for cross-species stromal cell types, identifying cell states specific for regenerative or fibrotic healing. While CRABP1+ fibroblasts are enriched in *Acomys* ears before and after injury, similar fibroblasts enriched in young, postnatal *Mus* ears remain unable to promote regeneration. Our data underscore the finely regulated dynamics of proliferating cells during regeneration and emphasize that regeneration depends on multiple factors including the presence of specific cell types and the ability of cells to acquire specific states.

68 **Key Conclusions:**

69 -Differentiated cells in *Acomys*, *Mus* and *Danio* re-enter the cell cycle in response to injury,
70 while homeostatic cycling cells contribute to blastema formation in *Ambystoma*

71 -Pulse-chase thymidine analog labeling shows tight spatiotemporal control of proliferating
72 stromal cells during regeneration in *Acomys*.

73 -Following injury, CRABP1 and αSMA are expressed in distinct stromal cell populations in
74 *Acomys* but are co-expressed in *Mus* stromal cell populations.

75 -Species-specific cell states underlie regenerative and fibrotic repair

76 -CRABP1+ cells are lost during embryonic development in *Mus* ear pinna but are retained in
77 *Acomys* to adulthood.

78 -Young neonatal *Mus* with abundant CRABP1+ cells still fail to execute regenerative healing

79

80

INTRODUCTION

Epimorphic regeneration is mediated by proliferating cells that form a blastema and subsequently differentiate to replace missing tissue (Morgan, 1901). Nearly all regenerative species use epimorphic regeneration to rebuild missing tissue. Seminal studies using urodeles, zebrafish, and planarians explored the dynamics of proliferating cells to understand their origin, proliferative rates, migration patterns, and responses to different injury types (Hays & Fischman, 1961; Poleo et al., 2001; Wallace, 1981; Wenemoser & Reddien, 2010). For example, thymidine analogs applied to amputated newt limbs revealed that cells start to synthesize DNA in differentiated tissues adjacent to the wound site (Hays & Fischman, 1961). These cells are then liberated and displaced distally to form the blastema. Similar studies in axolotls quantified cell cycle length, identified factors that maintain proliferation, and blocked proliferation to study regeneration (Maden & Wallace, 1976; Wallace, 1981; Wallace & Maden, 1976). In planarians, different injury types trigger distinct mitotic responses. For example, amputation causes local and systemic responses, while injuries that do not remove tissue only trigger a systemic response (Wenemoser & Reddien, 2010). Similarly, zebrafish regeneration studies have characterized the spatiotemporal distribution of proliferating cells across the blastema (Nechiporuk & Keating, 2002; Poleo et al., 2001). Considering these studies, an open question is the degree to which patterns and processes governing cell proliferation may hold during instances of epimorphic regeneration in mammals.

Complex tissue regeneration in vertebrates has been primarily studied in fishes, amphibians and invertebrates. However, some mammals exhibit bona fide regeneration (Billingham et al., 1959; Borgens, 1982; Carlson, 2005; Gawriluk et al., 2016; Goss & Grimes, 1972; Neeham, 1953; Seifert et al., 2012; Vorontsova et al., 1960). For instance, patterned musculoskeletal tissue is reconstituted after removal with a full thickness hole punch through the ear pinna in some lagomorphs and deomyine rodents (e.g., *Acomys* and *Lophuromys*) (Gawriluk et al., 2016; Goss, 1980; Goss & Grimes, 1972; Joseph & Dyson, 1966; Riddell et al., 2025; Seifert et al., 2012). Comparative studies between regenerative and non-regenerative rodents showed that spiny mice (*Acomys*) can regenerate ear pinna tissue after full thickness excisional injury; a response mediated by cell proliferation and blastema formation. In response to an identical injury, however, laboratory mice (*Mus*) cannot regenerate missing tissue and while cells

112 are activated to re-enter the cell cycle in response to injury, these cells are arrested shortly
113 afterwards (Gawriluk et al., 2016; Seifert et al., 2012).
114 In adult mammals, cell division is generally restricted to stem and progenitor cells in
115 tissues that require constant turnover during homeostasis (Cheung & Rando, 2013; Liu et al.,
116 2019; Orford & Scadden, 2008). In highly regenerative mammals, are there certain cell types or
117 states that can specifically re-enter the cell cycle and proliferate? In highly regenerative
118 vertebrates, blastema formation appears to be supported by cellular re-programming (aka
119 dedifferentiation) of lineage-restricted progenitors located near the wound site (Echeverri et al.,
120 2001; Gerber et al., 2018; Jopling et al., 2010; Leigh et al., 2018). Interestingly, while lineage-
121 restricted progenitors undoubtably support mouse digit tip regeneration (G. L. Johnson et al.,
122 2020; Lehoczky et al., 2011; Rinkevich et al., 2011), the capacity of mesenchymal cells to
123 maintain a specific transcriptomic state is also associated with regeneration (Storer et al., 2020).
124 Similar observations come from research comparing injured deer antler velvet (regenerative) to
125 dorsal back skin (non-regenerative) where both skin types have *Acta2*+ myofibroblast cells, but
126 specific transcriptomic profiles in these cells are associated with location. Importantly, velvet
127 fibroblasts access regulatory networks skewing them towards an immunosuppressive, pro-
128 regenerative fetal phenotype, while back skin fibroblasts express networks related to an
129 inflammatory, pro-fibrotic outcome (Sinha et al., 2022). Wound healing studies in large skin
130 wounds that regenerate hair follicles are biased to use a specific fibroblast subtype that is
131 inhibited in fibrotic responses; a finding that is also associated with better healing outcomes in
132 neonatal *Mus* and human skin (Guerrero-Juarez et al., 2019; Mine et al., 2008; Phan et al.,
133 2021a). Together, these studies support that access to regenerative cell states ***and*** the presence of
134 specific cell types is essential to promote a regenerative outcome.
135 Here we use the spiny mouse ear pinna regeneration model compared to fibrotic repair of
136 identical injuries in laboratory mice to explore the spatiotemporal dynamics of proliferating cells
137 and begin identifying cell types that participate in regeneration. First, we use a pulse-chase
138 method to quantify cell cycle activation in regenerative vertebrates with determinate and
139 indeterminate growth and find that growth mode is not strictly associated with regenerative
140 ability or the lack thereof. Additionally, we find no evidence of long-range cell activation in
141 response to injury. Using a pulse-chase labeling strategy in *Acomys*, we show that proliferating
142 cells maintain a distal position relative to the wound site, while cells in the proximal

143 compartment exit the cell cycle and differentiate. Finally, using a combination of
144 immunostaining and scRNA-sequencing, we identify similar cell types across species that
145 express distinct transcriptomic states associated with regenerative or fibrotic repair supporting
146 that species-specific cell states underlie regeneration and scaring.
147
148 **METHODS**
149
150 **Animal care**. Sexually mature, spiny mice (*Acomys dimidiatus* - aged six months to one year
151 old) and *Mus musculus*, ~three months old) were obtained from our in-house breeding colonies
152 at the University of Kentucky. Animals were maintained on a 12:12 h L:D light cycle. Both
153 species were fed 14% mouse chow (Teklad Global 2014, Harlan Laboratories) and *Acomys* diets
154 were supplemented with black sunflower seeds. All animal experiments were approved by
155 University of Kentucky Institutional Animal Care and Use Committee (IACUC) under protocol
156 2013–3254.
157
158 **4mm ear punch assay regeneration assay**. A 4mm full thickness excisional punch through the
159 ear pinna serves as a tissue regeneration assay (Gawriluk et al., 2016). Animals were
160 anesthetized with 3% vaporized isoflurane (v/v) (Henry Schein Animal Health, Dublin, OH) at 1
161 psi oxygen flow rate. A 4mm biopsy punch (Sklar Instruments, West Chester, PA) was used to
162 create a through-and-through hole in the right and left ear pinna. Ear tissue was collected at
163 specified time points using an 8mm biopsy punch (Sklar Instruments, West Chester, PA)
164 circumscribing the original injury. The published protocol can be found here:
165 dx.doi.org/10.17504/protocols.io.bp2l6dx65vqe/v1.
166
167 **Pulse-chase experiments**. We injected Ethynyl deoxyuridine (EdU) (10 ug/g) and
168 Bromodeoxyuridine (BrdU) (1 ug/g) diluted in normal saline, for pulse-chase experiments to
169 label and track cycling cells (the published protocol can be found here:
170 dx.doi.org/10.17504/protocols.io.261gerdmol47/v1). Both solutions were injected
171 intraperitoneally with a difference of five days between the EdU and BrdU injections. EdU and
172 BrdU injections were given as three separate injections, one every three hours over a period of
173 nine hours. The left ear pinna was collected after the EdU pulse to assess baseline cell numbers

174 in S-phase, and the right pinna was collected after the BrdU pulse to track single (EdU+ or
175 BrdU+) and double positive cells. The injection scheme was as follows: the first group of
176 animals was injected with EdU at D0 and BrdU at D5, the next group was injected with EdU at
177 D5 and BrdU at D10 and so on until D30. Hence, tissue samples were collected at 0, 5, 10, 15,
178 20, 25, and 30-days post injury.
179 Our experimental scheme allowed us to distinguish cells that (i) were in S-phase at the
180 time of the EdU injections and stopped proliferating within next five days (Edu+ alone); (ii) were
181 in S-phase at the time of the EdU injections, divided multiple times over five days diluting the
182 EdU, and remained in the cell cycle acquiring BrdU (weak EdU+/ strong BrdU+) - because each
183 cell division dilutes the EdU by half, a scenario where EdU is not detectable is possible, and
184 these cells would contribute to the BrdU+ alone counts); (iii) cells not in S-phase during the EdU
185 pulse but were cycling during the BrdU injections (BrdU+ alone); (iv) cells that acquired EdU,
186 divided only a few times, and remained in the cell cycle during the BrdU chase (strong EdU+/
187 strong Brdu+).
188
189 **Histology, EdU detection and Immunohistochemistry**. Harvested tissue was fixed
190 overnight in 10% neutral buffered formalin (NBF) (Thermo Fisher Scientific Inc. Epredia
191 5701) at 4˚C on a shaker. After 16-20 hrs the tissue was washed 3x with PBS, 3 minutes
192 per wash, followed by 3x 70% ethanol washes for dehydration and storage at 4˚C. Stored
193 tissue was processed for paraffin (Leica Biosystems, Buffalo Grove, IL, Formula "R"
194 REF: 3801450) embedding using a Histo5 tissue processor machine (Milestone). Samples
195 were sectioned at 5µm. EdU was detected using click chemistry as follows: Tissue
196 sections were de-paraffinized and rehydrated. Antigen retrieval was performed if co-
197 stained with antibodies. Tissues were washed two times for 10 minutes in Tris-buffered
198 saline (TBS) to incubate in the prepared reaction cocktail (see table below) for 30
199 minutes at RT protected from light. Tissues were washed two times in TBS for 5 minutes
200 and if co-stained with antibodies were blocked following the fluorescent IHC protocol for
201 BrdU and cell type specific antibodies tissue sections were deparaffinized and re-
202 hydrated. Tissues were then exposed to high heat antigen retrieval in a steamer in antigen
203 unmasking TRIS or citric acid-based solutions (Vector Laboratories, Inc.). After a 5-
204 minute wash, tissues were blocked in blocking serum (see table below) for 30 minutes at

205 RT. Tissues were then incubated with primary antibody diluted in blocking serum at 4 ˚C
206 overnight. After a 5 minutes wash, tissues were incubated in secondary antibody diluted
207 in blocking serum for 30 min at RT. Tissue samples were incubated with Hoechst 33342
208 for 5 minutes at RT and then dried and mounted in Prolong. Finally, protein similarity
209 was compared to assess antibody binding efficacy (Supplementary table S1). For
210 complete protocol details regarding paraffin sections
211 (dx.doi.org/10.17504/protocols.io.6qpvr9353vmk/v1), immunohistochemistry
212 (dx.doi.org/10.17504/protocols.io.n92ldrmd8g5b/v1), and EdU detection on sections
213 (dx.doi.org/10.17504/protocols.io.e6nvwbdrzvmk/v1).
214

EdU reaction cocktail	
Components	**Volume (ul)**
2 M Tris, pH 8.5	5
50 mM CuSO4	2
0.5 M ascorbic acid	20
Alexa fluor azide (0.25 mg/ml)	0.2
ddH2O	73
Total	100

215

Primary Antibodies					
Antibody	**Company, Cat#**	**RRID**	**Host species**	**Dilution**	**Antigen retrieval**
Anti-BrdU (Bromodeoxyuridine)	Abcam, Ab6326	AB_305426	Rat	1:500	Citric Acid
Anti-wide spectrum Cytokeratin	Abcam, Ab9377	AB_307222	Rabbit	1:500	None
Anti-ionized calcium-binding adapter molecule 1 (IBA1)	Novus Biologicals, NB100-10288s	AB_521594	Goat	1:400	Tris
Anti-retinoic acid-binding protein 1 (CRABP1)	Cell Signaling Technology, Inc, 13163	AB_2750569	Rabbit	1:500	Tris
Anti- alpha-Smooth Muscle Actin (alpha-SMA)	Novus Biologicals, NB300-978	AB_2273628	Goat	1:200	Tris

Anti-SRY Box Transcription Factor 9 (SOX9)	Abcam, ab185230	AB_2715497	Rabbit	1:1000	None
Anti-macrophage mannose receptor (MMR) (CD206)	R&D Systems, AF2535	AB_2063012	Goat	1:500	Tris

Secondary Antibodies				
Antibody	**Company, Cat#**	**RRID**	**Host species**	**Dilution**
Alexafluor 594 anti-Rabbit	Thermo Fisher Scientific, A21207	AB_141637	Donkey	1:400
Alexafluor 647 anti-goat	Thermo Fisher Scientific, A21447	AB_2535864	Donkey	1:400
Alexafluor 647 anti-rat	Thermo Fisher Scientific, A21247	AB_141778	Goat	1:400

Western Blotting. Protein extraction and quantification was performed as indicated (dx.doi.org/10.17504/protocols.io.rm7vzkx12vx1/v1). Western blotting was performed as indicated (dx.doi.org/10.17504/protocols.io.kqdg3qxz1v25/v1).

Imaging and Cell Quantification. Fluorescent images were collected using Cells Sens from Olympus in Olympus inverted microscope (Olympus America Inc). Whole tissue sections were captured in 20X and stitched automatically. Cell counting was manually performed in defined areas of the images separately in each channel using ImageJ. Percentages of positive cells were calculated by quantifying nuclei (Hoechst 33342) using the threshold tool in ImageJ.

Statistics. Statistical analyses were performed using JMP (version Pro 15.0, SAS Institute Inc) and SPSS (version 28.0, IBM) where alpha was set at 0.05 for all statistical analyses. Graphs were made in excel and JMP. To analyze our pulse chase data across species, we performed Two-way ANOVAs with either EdU+, BrdU+ or double positive cells (dependent variable), and days post injury (independent variable) followed by Tukey HSD multiple comparisons to test for differences in positive cells as a function of time (Supplementary table S2).

To analyze proliferation during regeneration in *Acomys*, we used a linear mixed model to assess differences in percentage of positive cells between three positions (A, B, C) over time

236 (D5-D30) (Supplementary table S3). Likelihood ratio testing and Akaike Information Criterion
237 (AIC) were used to select an appropriate covariance structure. A Kenward-Roger adjustment was
238 used to correct for negative bias in the 170 standard errors and degrees of freedom calculations
239 induced by the small sample size. Relevant pairwise comparisons were performed and controlled
240 for multiple comparisons using Fisher's Least Significant Differences (LSD). Mixed modeling
241 analysis was performed using SAS 9.4 (SAS Institute, Inc.; Cary, NC, USA).
242
243 **Single-cell analysis**. scRNA-seq data used in this study were download and available through
244 the Gene Expression Omnibus (GEO) (RRID:SCR_005012) under the accession number
245 GSE182141. The raw fastqs were processed through the CellRanger pipeline v8.0.1
246 (RRID:SCR_017344) using 10X Genomics' mm10-2020-A reference genome or a custom
247 annotated *Acomys dimidiatus* genome (GCA_907164435.1 (mAcoDim1_REL_1905), with the
248 'include introns' set to true to obtain gene expression matrices.
249 Background reads were removed using decontX from the celda package using the filtered
250 barcodes as the cells to keep and the remaining cells in the raw barcode matrix as the background
251 (Campbell et al., 2024). Doublets were minimized using DoubletFinder (RRID:SCR_018771)
252 (McGinnis et al., 2019). The R v4.4 (RRID:SCR_001905) library Seurat v5.1
253 (RRID:SCR_016341) (Hao et al., 2021; Hao et al., 2024)) was used for cell type clustering and
254 marker gene identification. Cells expressing >500 genes were retained for downstream analysis.
255 Each sample was normalized SCTransform v2 (RRID:SCR_022146), using the glmGamPoi
256 method and the number of RNA molecules per cell were regressed out. Samples were integrated
257 with common anchor genes using the CCA method to minimize sample to sample variation. Cell
258 clusters were determined by the Louvain algorithm using a resolution of 0.3. UMAP dimension
259 reduction was done using the first thirty principal components. Marker genes for each cell type
260 were calculated using the Wilcoxon Rank Sum test returning only genes that are present in a
261 minimum of 25% of the analyzed cluster. Cross species markers were done as above in cell types
262 of interest, but the pct.2 score was filtered to be > 0 to eliminate uniquely annotated genes from
263 dominating the lists. Volcano plots were created with the Enhanced Volcano (Blighe et al., 2024)
264 R library using the avg_log2FC and p_val_adj values as inputs.

265 Gene ontology (GO) analyses were performed in the Enrichr platform
266 (https://maayanlab.cloud/Enrichr/). Only differentially expressed genes with a two-fold change
267 were included in the analysis of GO Biological Process.

268

269 **RESULTS**

270

271 ***Vertebrate stromal cells rapidly re-enter the cell cycle in response to injury***

272 Notably few regeneration papers using salamanders or fish have indicated whether
273 stromal cells are proliferating during normal homeostasis. To explore proliferation in uninjured
274 tissue, we used EdU to label cells in S-phase in two highly regenerative amniotes (*Danio rerio* -
275 zebrafish, *Ambystoma mexicanum* - axolotl), in an adult mammal with enhanced regenerative
276 ability (*Acomys dimidiatus* – spiny mouse) and in a poorly regenerating mammal (*Mus musculus*
277 – outbred ND4 laboratory mouse strain) (Fig. 1A). Examining the ear pinna (*Acomys* and *Mus*),
278 limb (*Ambystoma*) and caudal fin (*Danio*), we found cycling cells in the epidermis from all four
279 species prior to injury; a finding that was expected given the presence of slow cycling stem cells
280 in the epidermis (Fig. 1B). In uninjured *Danio* and *Ambystoma* tissue, we also found a small
281 percentage of cycling cells in the stroma (1% and 0.5% respectively) supporting previous reports
282 for these species (Fig. 1B-C) (K. Johnson et al., 2018; Simkin & Seifert, 2018). In contrast, we
283 found only one or two cycling stromal cells across entire tissue sections in *Acomys* or *Mus* prior
284 to tissue removal (Fig. 1B-C). These data support that stromal cell proliferation is essentially
285 non-existent prior to injury in mammals, at least in the ear and skin.

286 A longstanding hypothesis is that cells in mammals are refractory to cell cycle re-entry
287 and progression whereas cells in highly regenerative vertebrates easily re-enter the cell cycle and
288 proliferate to replace missing tissue (Pajcini et al., 2010; Simkin & Seifert, 2018; Tanaka et al.,
289 1997; Tanaka & Brockes, 1998). To test this hypothesis, we used a pulse chase strategy whereby
290 we injected animals with EdU, performed the specified injury, injected BrdU at either 15 or
291 63hrs post injury (hpi) and then harvested tissue 9hrs later at 24 and 72 hpi (see Methods). We
292 quantified stromal cells that were EdU+, or BrdU+, or EdU+/BrdU+ (double positive) (Fig. 1B,
293 D). 24 hpi spiny mice and zebrafish showed the highest percentage of newly cycling cells in
294 response to injury (BrdU+). *Mus* cells also re-entered the cell cycle, albeit later at 72 hpi. Axolotl
295 limb tissue, on the other hand, exhibited very few singly BrdU+ cells but presented the highest

296 number of double positive cells (Fig. 1D). These data demonstrate that stromal cells in *Acomys*,
297 *Mus* and zebrafish re-enter the cell cycle *de novo* in response to injury with a 48hr lag observed
298 for *Mus* cells.
299 To assess cell activation arising from the injury but independent of the local repair
300 response (i.e., systemic cell activation), we collected the contralateral ear pinna in *Mus* and
301 *Acomys*, the contralateral limb in axolotls, and the pelvic fin in zebrafish 24 hpi and 72 hpi after
302 tissue amputation. Using a pulse chase strategy as described above, we looked for cell cycle re-
303 entry in uninjured tissues at 24 hpi and 72 hpi. EdU+ cells were cycling prior to injury, BrdU+
304 cells were those activated systemically and EdU+/BrdU+ were those cycling prior to injury that
305 were activated systemically. Despite reports in lab mice of long-range cell activation in skeletal
306 muscle stem cells (Rodgers et al., 2014), in *Acomys* and *Mus*, we did not find a noticeable
307 response in the contralateral ear pinna where the number of BrdU+ cells did not exceed 0.5% at
308 either time point (Fig. S1A-B). Similarly, in axolotl and zebrafish, the number of EdU+ cells at
309 24 and 72 hpi was similar to the number of positive cells found in uninjured tissue at D0 (see
310 above) (Fig. S1A-B). These data indicate that a systemic response to injury is negligible at 24
311 and 72hpi in all four species.
312
313 ***Proliferating cells are maintained in a distal position relative to the wound site over time***
314 *Acomys* species regenerate ear pinna tissue after removal with a 4 mm (or larger) biopsy
315 punch whereas identical tissue excisions in wild or laboratory *Mus* result in scar tissue formation
316 (Seifert et al., 2012). To more thoroughly understand the kinetics of proliferating cells during
317 regeneration and fibrotic repair, we again employed a pulse (EdU) chase (BrdU) scheme where
318 our pulse and chase were separated by a five-day window (see Methods). First, we analyzed
319 BrdU+ cells to estimate the proliferative rate from injury until D30 and then analyzed the spatial
320 distribution of cycling cells by quantifying cells adjacent to the injury (aka proximal) and at two
321 distal locations (i.e., closest to the new epidermis); distal dorsal and distal ventral (Fig. 2A-E).
322 We quantified healing tissue area from D10-30 which supported continued addition of new tissue
323 during regeneration (Fig. 2B). In contrast, after a proliferative burst, no new fibrotic tissue was
324 added in *Mus* ears after D10 (Fig. 2C).
325 Analyzing BrdU+ cells during regeneration revealed that from D15 to D30, the number
326 of cycling cells was significantly higher in the distal areas compared to the proximal areas

327 (injury site) while there was no difference between the distal-dorsal and distal-ventral areas (Fig.
328 2D and Supplementary Table 1). An exception was D20 when the new tissue areas were small or
329 flat and thus distal and proximal areas were close (Fig. 2D). While cell proliferation in the
330 proximal compartment decreased over time, proliferation in the distal compartment remained
331 >10% from D10-30 contributing to the steady production of new tissue. (Fig. 2D). Quantifying
332 BrdU+ cells in *Mus* ears, we observed a narrow extension of new tissue (Fig. 2A). After a burst
333 of DNA replication (>25%) in *Mus* at D5, the percent of BrdU+ cells precipitously declined from
334 D10-30 coinciding with no increase in tissue area over this time period (Fig. 2C, E).
335 To assess the spatial distribution of cycling cells during regeneration (D10-30), we first
336 analyzed the epidermis where stem cell localization and proliferation are well known. Basal stem
337 cells in the deeper layer of the epidermis show symmetrical and asymmetrical cell division
338 depending on whether they produce progeny or more stem cells (Blanpain & Fuchs, 2006).
339 Analyzing our pulse-chase data, we observed stem, progenitor, and differentiating cells in the
340 epidermis (Fig. S2A-B). The stratum basale contained slow-cycling stem cells (strong EdU+)
341 and infrequently dividing stem cells (EdU+/BrdU+) while also indicating rapidly-cycling
342 progenitor cells (strong BrdU+/diluted EdU+), and recently-cycling progenitor cells (strong
343 BrdU+ Fig. S2A-B). In addition, we observed progenitor cells having acquired EdU that
344 migrated apically withdrawing from the cell cycle and undergoing differentiation as per the
345 absence of BrdU (Fig. S2B, yellow arrow). These cell behaviors demonstrated that our labeling
346 scheme could effectively capture predicted stem cell behavior in a tissue with known
347 proliferative properties.
348 Next we characterized proliferative behavior in the stromal compartment by quantifying
349 cells that re-entered the cell cycle after injury but arrested within five days (EdU+ only) possibly
350 to differentiate or re-enter the cell cycle later (slow-cycling progenitors), and cells that re-entered
351 the cell cycle but maintained their proliferative state over the same period (EdU+/BrdU+ and
352 BrdU+ only) in both distal and proximal areas relative to the wound site (Fig. 2F-I). We
353 hypothesized that cell proliferation could either be clonal, with multiple daughter cells near
354 proliferative progenitors in rosettes or could expand from the wound site. In the latter case, we
355 predicted to capture progenitors cycling near the wound margin and daughter cells building up
356 the blastema distally. At D10, we found a stochastic pattern of proliferation with a mixture of
357 EdU+ cells, BrdU+ cells, and double-positive cells in distal and proximal compartments, where

358 the EdU+ cell population represented the biggest population (>25%) (Fig. 2F-G). At D25,
359 however, we were able to observe a pattern where rapid-cycling (BrdU+) and infrequently-
360 dividing (double positive) cells represented half of the proliferative population (>9%) in the
361 distal compartment with the other half (~8%) being represented by potentially slow cycling
362 progenitors (EdU+) (Fig. 2H-I). In comparison, the proximal area was represented mostly by
363 EdU+ cells (5%) that may have started differentiation and a very small percentage of rapid-
364 cycling and infrequently-dividing (1%) cells that could support expansion of some differentiating
365 cell types (Fig. 2H-I). Supporting this pattern, we observed differentiation of new hair follicles
366 and cartilage near the wound site. *In toto*, these results show that the proliferative progenitor
367 population is maintained in a distal position relative to the wound site. Furthermore, our pulse
368 chase labeling supports cell cycle progression and asynchronous cell proliferation during
369 regeneration in *Acomys*, whereas thymidine analog incorporation without cell division was
370 observed in *Mus*, suggesting an S-phase arrest after D10.
371
372 ***The proliferative population comprises diverse cell types in Acomys***
373 To determine cell state or identity among the proliferative population (PP), we co-labeled
374 with cell type specific markers and EdU (see Methods). Although we found no mesenchymal cell
375 types proliferating in uninjured tissue, we characterized the distribution of macrophages
376 (IBA1+), chondroblasts (SOX9+) and two fibroblast subtypes (CRABP1+ or αSMA+) in
377 comparison with *Mus* to identify any obvious differences in presence and location across tissue
378 compartments (Fig. S3A-J). First, we found relatively few CD206+ and IBA1+ macrophages
379 (Fig. S3A, B, F, G) nor αSMA+ cells which were sparse (Fig. S3E, J). We observed two
380 populations of SOX9+ cells in both species: one associated with the perichondrium, and another
381 associated with the sebaceous gland and hair follicle (Fig. S3C, H). Importantly, we observed a
382 population of CRABP1+ fibroblasts scattered throughout the papillary dermis in *Acomy*s while
383 these cells were not detectable in uninjured *Mus* skin (Fig. S3D, I).
384 Examining these same cell types at D5, we observed cell-cycle re-entry among many of
385 them (Fig. 3A-J). By counting all the EdU+ cells in a counting frame and then quantifying
386 double positive cells we estimated the fraction of cycling cells represented by each cell type.
387 Because inflammation peaks at D5 (Gawriluk et al., 2020), we hypothesized that a large fraction
388 of proliferating cells would be macrophages. Instead, IBA1+ and CD206+ cells represented only

389 5.3% and 4.95% of the PP respectively in *Acomys* and 5.3% and 0.96% in *Mus* (Fig 3A-D). In
390 *Acomys*, the two fibroblast subtypes (CRABP1+ and αSMA+ cells) represented ~14% and
391 18.65% respectively while chondroblasts (SOX9+ cells) represented ~16% of the PP in *Acomys*
392 (Fig. 3E, G, H). Surprisingly, although totally absent prior to injury in *Mus*, an emergent
393 CRABP1+ population represented 28.9% of the PP at D5 (Fig. 3I). SOX9+ and αSMA+ cells
394 represented 7.96%, and 33% of the PP in *Mus* (Fig. 3F, J). These data support that various cell
395 types re-enter the cell cycle during regeneration *and* fibrotic repair.
396 Only *Acomys* maintains a proliferative population during regeneration whereas activated
397 cells did not appear to maintain cell cycle progression or appreciably divide during fibrotic
398 repair. Co-staining with EdU, we confirmed the above-mentioned cell types remained part of the
399 PP at D20 in *Acomys* (Fig. 4A-C and Fig. S4A-B). Of note, we observed that CRABP1+,
400 αSMA+, and SOX9+ cells were segregated spatially throughout the blastema (Fig. 4A-C, G, H
401 and Fig. S5A). While the CRABP1+ population was restricted to the papillary dermis at D0, this
402 population expanded to deeper dermal areas at D5 (Fig. 3D, G and Fig. S5A) and occupied the
403 dorsal blastema with another, smaller population in the ventral papillary zone at D20 (Fig. 4A-
404 A', G-H and Fig. S5A). In contrast, the αSMA+ fibroblast population appeared after injury in a
405 distal and central position where reticular fibroblasts localize (Fig. 3H-H' and Figs. S3E, S5A).
406 This population shrunk at D20 and was largely non-overlapping with CRABP1+ cells (Fig. 4B-
407 B', G-H and Fig. S5A). Thus, as the blastema expanded, the αSMA+ fibroblasts maintained a
408 small, distal population that disappeared in proximal tissue, while the CRABP1+ population
409 expanded over time (Fig. 4G-H). In response to injury, the SOX9+ population that labeled the
410 perichondrium appeared in the blastema perfectly aligned with the cartilage (Fig. 4C and Fig.
411 S5A). IBA1+ and CD206+ cells were spread evenly across the blastema (Fig. S4A-B and Fig.
412 S5A).
413 The configuration of these populations was notably different in *Mus* during healing (Fig.
414 4D-F and Fig. S5B). Absent at D0, a CRABP1+ population emerged throughout the injury zone
415 at D5, only to become restricted to the distal tip of the ear at D20 with distinctly fainter antibody
416 reactivity (Figs. 3I & 4D and Fig. S5B). αSMA+ cells, absent in *Mus* at D0, became the
417 dominant population in distal scar tissue (Fig. 4E and Fig. S5B). We observed some Sox9+ cells
418 in the middle of the outgrowth (Fig. 4F and Fig. S5B), and IBA1+ and CD206+ cells distributed
419 widely throughout the scar tissue (Fig. S4C, D and Fig. S5B). Western blotting for CRABP1

420 supported our observations using immunohistochemistry (Fig. S5C). Together, these results
421 uncovered a distinct spatial segregation of cell types with a prominent CRABP1+ population
422 present in *Acomys* before and after injury, that was merely transient in *Mus*.
423
424 ***Species-specific cell states separate scaring and regeneration phenotypes***
425 To extend our cellular studies, we next interrogated a scRNA-seq dataset harvested from
426 uninjured (D0) and healing ear tissue at D3, 5, 10 and 15 from *Acomys* and *Mus* (Simkin et al.,
427 2024). Unbiased clustering of batch corrected data for all time points (see Methods) revealed the
428 same cell populations across species (Fig. S7). Thus, we extracted the four main stromal cell
429 populations, fibroblasts (cluster 18), chondroblasts (cluster 19), lymphatic endothelial cells
430 (cluster 16) and vascular endothelial cells (cluster 9), and generated a new UMAP (Fig. 5A). Re-
431 clustering revealed eight subpopulations among the four original stromal populations: two
432 populations each of vascular and lymphatic endothelial cells, three fibroblast subtypes, and a
433 single chondroblast population (Fig. 5B). To investigate markers from our immunohistochemical
434 analysis, we plotted *Crabp1*, *Acta2* (αSMA), and *Sox9* across cells on this UMAP (Fig. 5B).
435 Interestingly, we found that *Acta2* transcripts were strongly associated with one fibroblast
436 subtype (cluster 7) while *Crabp1* was totally excluded from this cluster (Fig. 5B-D). *Sox9*
437 marked chondroblasts in both species (Fig. 5E). To assess co-localization, we plotted *CRABP1*
438 and *Acta2* together and found few double positive cells in *Acomys* (Fig. S8A). In contrast,
439 fibroblast cluster six was mostly double-positive for *Crabp1* and *Acta2* in *Mus* (Fig. S8B). In
440 addition, fibroblast cluster four and lymphatic endothelial cluster five were heavily enriched for
441 *Acta2* in *Mus* (Fig. S8B). These data support a distinct *Acta2*+ fibroblast population in both
442 species (cluster 7) and a *Crabp1*+ fibroblast subtype in *Acomys* that is *Acta2*-. In *Mus*, *Crabp1*
443 appears to only mark a transitional cell state that ultimately expresses *Acta2* while *Acta2*
444 generally increases among fibroblasts and lymphatic endothelial cells supporting a fibrotic
445 phenotype in *Mus*.
446 To better understand intrinsic differences between the fibroblast subpopulations, we ran
447 differential gene expression (DGE) analysis comparing the three *Acomys* fibroblast clusters
448 against the three *Mus* clusters (Fig. 5F-K). This analysis revealed 1497 genes (488 in *Acomys*,
449 1009 in *Mus*) differentially upregulated in cluster four, 1228 (510 in *Acomys*, 718 in *Mus*) in
450 cluster six, and 743 (248 in *Acomys*, 495 in *Mus*) in cluster seven among both species (Fig 5F, H,

451 J). Gene ontology of each cluster separated by species revealed a clear segregation in the
452 fibroblast response to injury (Supplementary Table S4). The three fibroblast populations in *Mus*
453 were associated with fibrotic pathways: response to TGFß stimulus, cellular response to hypoxia,
454 and negative regulation of epithelial cell proliferation, among others (Fig 5G, I, K). In contrast,
455 *Acomys* subpopulations were associated with telomere maintenance and cell proliferation
456 pathways (Fig 5G, I, K). Interestingly, *Acta2*-expressing cluster seven was associated with
457 regulation of fat cell differentiation, positive regulation of translation and regulation of
458 membrane protein ectodomain proteolysis (Fig 5K). Chondroblasts (cluster two) followed a
459 similar pattern with 2234 genes (786 in *Acomys*, 1448 in *Mus*) differentially upregulated. *Acomys*
460 chondroblasts upregulated genes associated with translation, response to hydrogen peroxide and
461 gene expression, while *Mus* chondroblasts upregulated genes associated with TGFß stimulus and
462 regulation of TGFß-Receptor signaling (Fig. S9B). Of note, all four clusters (two, four, six and
463 seven) in *Acomys* highly upregulated *Zc3h10* and *Tssc4* (Fig. 5F, H, J and fig. S9A). The first
464 gene has been shown to boost mitochondrial function (Audano et al., 2018), while the second
465 gene promotes cell survival and proliferation in breast cancer tumors (Chen et al., 2022).
466 Together, these data show that all four *Mus* subpopulations activate fibrosis-related
467 pathways, while the four subpopulations in *Acomys* are biased toward pathways associated with
468 cell proliferation and growth. Importantly, while the same markers may be able to identify
469 fibroblast subtypes in both species, the intrinsic ability of each subtype to respond to injury
470 differs.
471
472 ***CRABP1+ fibroblasts do not induce regeneration in neonatal Mus.***
473 Previous studies using very large wounds in lab mice observed hair follicle regeneration
474 in the wound center, an observation that has been attributed to the presence of *Crabp1+*
475 fibroblasts (the so-called WIHN model) (Jiang & Rinkevich, 2021; Phan et al., 2021b). Since we
476 did not observe CRABP1+ cells in uninjured *Mus* tissue, but did observe them in *Acomys* ear
477 dermis prior to injury and during regeneration, we hypothesized these cells disappear during *Mus*
478 ear development. To test this hypothesis, we assessed CRABP1 reactivity in embryonic,
479 neonatal, juvenile and adult ear tissue (Fig. 6A). In *Acomys,* we found CRABP1+ reactivity
480 across all stages (embryonic and neonatal) and into adulthood (8 months old) (Fig. 6A).
481 CRABP1 reactivity was strongest at embryonic stages and restricted to the dermis where it

482 persisted into adulthood; mainly the papillary dermis (Fig. 6A). In contrast, we found *Mus*
483 fibroblasts started to lose CRABP1 expression around P20 and it was totally absent from the ear
484 pinna in three month old adults (Fig. 6A).
485 Based on these observations, we hypothesized that challenging *Mus* ear pinnae using our
486 regeneration assay in the presence of CRABP1+ fibroblasts might enhance ear hole regeneration.
487 Performing a 4 mm ear punch in P20 animals, we found neonatal ear holes produced tissue until
488 D15 (Fig. 6B-C), but did not close. Similarly, we performed 2 mm punches in P23 animals and
489 did not observe regeneration (Fig. S10A-B). Next, we injured P15 *Mus* which have CRABP1+
490 fibroblasts and collected tissue at D5 and D20. CRABP1 reactivity after injury was similar to
491 that observed in adult *Mus* with increased expression at D5 which disappeared by D20 (Fig 6D).
492 Again, we did not observe regeneration. Together, these data show the presence of a CRABP1+
493 fibroblast population is not sufficient to promote a regenerative response and instead supports
494 species-intrinsic adoption of cells states that support regeneration.
495
496
497 **DISCUSSION**
498 Here we conducted a comprehensive analysis of cell proliferation during regeneration
499 and found cycling cells maintained a distal position relative to the original injury, while proximal
500 cells exited the cell cycle and differentiated. These data revealed controlled regulation of the cell
501 cycle in response to injury such that while amputation served as an activation trigger in both
502 species, regenerating tissue maintained cell cycle progression while cells participating in fibrotic
503 repair arrested. Importantly, proliferation in *Acomys* did not lead to tissue overgrowth
504 demonstrating regulated shutdown of cell cycle progression. This unites *Acomys* with other
505 highly regenerative vertebrates where tightly controlled cell proliferation is a hallmark of
506 epimorphic regeneration in zebrafish caudal fins (Nechiporuk & Keating, 2002; Poleo et al.,
507 2001) and newt limbs (Hays & Fischman, 1961; Wallace & Maden, 1976). Cell proliferation in
508 injured mammalian organ stroma, apart from dedicated stem cell populations, is rarely observed
509 except during tumorigenesis where cell proliferation is uncontrolled (Hanahan & Weinberg,
510 2011).
511 Although evolutionary explanations for the presence of regenerative ability among some
512 vertebrate clades remains poorly supported, the presence of indeterminate growth has been

513 offered as an underlying prerequisite (Froehlich et al., 2013; Sebens, 1987). This hypothesis
514 claims that indeterminate growers maintain populations of somatic stem or progenitor cells that
515 behave like slow-cycling stem cells to support growth. There are two arms to this hypothesis.
516 First is the presence of cycling somatic cells during homeostasis lowers the barrier to cell cycle
517 re-entry upon injury. Second is that once cycling, cells do not activate tumor suppressor
518 machinery during S-phase progression to initiate cell cycle arrest. These ideas partly stem from
519 culture experiments with newt myotubes that easily re-enter the cell cycle after serum
520 stimulation in contrast to mouse myotubes formed from C2C12 cells which are refractory to cell
521 cycle re-entry (Tanaka et al., 1997; Tanaka & Brockes, 1998). Although *Mus* myotubes can be
522 forced to re-enter the cell cycle, this requires deletion or inactivation of tumor suppressors
523 retinoblastoma protein (pRB) and $p16^{ink4a}$ (Gu et al., 1993; Schneider et al., 1994).
524 To examine if cycling somatic cells exist in highly regenerative vertebrates, we analyzed
525 cell cycle re-entry and progression prior to and after injury between determinate (*Acomys*, *Mus*)
526 and indeterminate growers (*Ambystoma* and *Danio*). In line with previous observations (K.
527 Johnson et al., 2018; Simkin & Seifert, 2018), we found a small population of slow-cycling
528 stromal cells present during homeostasis in indeterminate growers while we failed to detect these
529 cells in determinate growers. This cycling population, however, scarcely contributed to blastema
530 formation in zebrafish. Instead, cells that re-entered the cell cycle in response to injury were the
531 major contributors to regeneration. This result supports a previous study in zebrafish where slow-
532 cycling cells marked for eight weeks before injury did not contribute to blastema formation
533 (Nechiporuk & Keating, 2002). Importantly, our data show that cells in *Acomys* and *Mus* re-enter
534 the cell cycle in response to injury independent of their regenerative ability. An open question is
535 how cell cycle progression is controlled for almost forty days and then downregulated so as not
536 to create tissue overgrowth. Considered *in toto*, our cross-species analysis rejects the notion that
537 a determinate growth mode prevents cell cycle re-entry and supports that the contribution of
538 slow-cycling cells to the blastema is minimal, at least in fish.
539 Our cross-species proliferation experiments also assessed whether cells on the other side
540 of the animal were activated by injury (so-called systemic cell activation). Work in lab mice
541 found that acute muscle injury elicits a systemic response in which contralateral-located stem
542 cells (CSCs) re-enter the cell cycle and access a priming state named G_{Alert} (Rodgers et al.,
543 2014). In contrast to quiescent stem cells (QSCs), CSCs in mouse show an increased propensity

544 to cycle, although their numbers remain low in comparison with stem cells located at the injury
545 site (Rodgers et al., 2014). A similar systemic response was observed in axolotl limbs
546 contralateral to amputated limbs (Johnson et al., 2018). Using contralateral control tissue
547 collected in our experiments, we looked for primed cells *in vivo* following injury. In contrast to
548 muscle stem cells in *Mus*, we found a negligible stromal response in *Acomys* and *Mus* with less
549 than 0.5% of contralateral ear pinna cells responding to a systemic signal. While we used
550 immunofluorescence to quantify active or primed mesenchymal cells in tissue sections, previous
551 studies in mouse muscle used FACS sorted satellite stem cells to assess *in vivo* BrdU
552 incorporation. Supporting our observations in *Acomys* and *Mus*, we could not find a significant
553 response in contralateral axolotl limbs or zebrafish pelvic fins, at least in the first 72hrs after
554 injury. While these results are at odds with a single axolotl study, those data included epidermal
555 cells in their cell counts and later time points (Johnson et al., 2018). Thus, our data do not
556 support significant stromal cell cycle re-entry in uninjured contralateral tissue from the four
557 species analyzed.
558 Contemporary vertebrate regeneration studies using transgenics have concluded that
559 blastemas particular to an injured tissue are formed from a heterogeneous population of cells at
560 the amputation plane (rev. in Seifert & Muneoka, 2018). Although various stem cell reservoirs
561 have been discovered in different mammalian tissues, except for the digit tip, exploring cell type
562 contributions during complex tissue regeneration in mammals has been impossible. While we
563 could not identify stem cells with our methods, our data support that *Acomys* expands pre-
564 existing cell types to participate in regeneration via cell proliferation. One exception in our
565 analysis were αSMA+ fibroblasts which appeared after injury but did not maintain αSMA
566 identity in newly differentiated tissue. Interestingly, our scRNA-seq data indicated that an *Acta2*-
567 expressing population expressed genes related to the regulation of fat cell differentiation
568 suggesting that some myofibroblasts may differentiate into adipocytes in a regenerative context.
569 Similarly, αSMA+ myofibroblasts were shown to differentiate into adipocytes when exposed to
570 bone morphogenetic protein (BMP) triggered by neogenic hair follicles in large skin wounds
571 (Plikus et al., 2017). Further supporting our observations, recent data from another *Acomys* ear
572 pinna regeneration study reported that αSMA fibroblasts disappear after wound closure with
573 only ACTA2+ vascular smooth muscle cells remaining (Brewer et al., 2021). We too observed
574 high expression of TGFβ pathway components in *Mus*, but not *Acomys* fibroblasts. Taken with

575 the previously observed insensitivity of *Acomys* fibroblasts to TGFβ induced myofibroblast
576 differentiation (Brewer et al., 2021), *Acomys* appears to support reduced myofibroblast
577 activation. While these data suggest a possible differentiation trajectory for myofibroblasts, the
578 exact dynamics of αSMA+ cells await further study in a regenerative context.
579 In contrast to their role during regeneration, the role of myofibroblasts during fibrotic
580 skin repair is well known (rev. in Plikus et al., 2021). Previous studies in skin have described
581 first wound responders as a large proportion of reticular fibroblasts including αSMA+ fibroblasts
582 (Driskell et al., 2013) which rapidly seal the wound area promoting scaring and inhibiting hair
583 follicle formation (Correa-Gallegos et al., 2019). These data support our observations in *Mus*
584 where αSMA+ fibroblasts are the main cell population in newly generated scar tissue. Together,
585 these data show that αSMA fibroblasts are dominant in scaring but seem to be transient in
586 regeneration.
587 CRABP1+ papillary fibroblasts abundantly participate in the regeneration of neonatal
588 skin and deer antler velvet and thus we interrogated their behavior in our ear pinna assay (Phan
589 et al., 2021b; Sinha et al., 2022). In contrast to the ephemeral nature of the αSMA+ population in
590 *Acomys*, we observed a stark difference in CRABP1+ cells during regeneration and fibrotic
591 repair. While we were unable to detect CRABP1+ cells prior to injury in *Mus*, these cells
592 appeared at D5 as a subset of cycling cells only to disappear by D20. In *Acomys*, however, we
593 detected CRABP1+ cells prior to injury and this population expanded to participate in blastema
594 formation. CRABP1 has been found in a variety of regeneration contexts. For instance, this
595 protein is expressed in *Mus* papillary fibroblasts that expand in large, somewhat regenerative
596 wounds (Guerrero-Juarez et al., 2019). Other examples are the regenerating wounds in newborn
597 (P2) mice that have a higher proportion of CRABP1+ fibroblasts (Phan et al., 2021a) and the
598 velvet skin on deer antlers which have regeneration-primed fibroblasts expressing genes
599 putatively associated with a regenerative phenotype (e.g., *CRABP1, RUNX1,* and *PRSS35*)
600 (Sinha et al., 2022).
601 Rather than the presence or lack of a specific cell type, our scRNA-seq data suggests that
602 it may also be one of cell state. Although all four stromal subclusters express some of the same
603 markers in *Acomys* and *Mus*, our DGE and GO analyses revealed that the four *Mus* subclusters
604 express biological processes related to fibrosis. In contrast, all four subclusters in *Acomys* seem
605 to use biological processes related with cell proliferation; high transcription and telomere

606 maintenance and genes that boost mitochondrial function and cell survival. Specifically, a
607 subpopulation in both species that highly expressed *Acta2* exhibited divergent transcriptomic
608 responses. Future studies are necessary to address whether *Acomys* αSMA+ cells transiently
609 become myofibroblast-like only to later differentiate into adipocytes as suggested by our GO
610 analysis. Our finding that two subpopulations expressed high telomerase and endoplasmic
611 reticulum stress (ERS) related activity supported the persistence of proliferation in these cells.
612 Telomerase activity is low in most non-proliferating somatic cells in humans and mice, while
613 high activity has been reported in highly proliferating immortal and cancer cells (Kim et al.,
614 1994; Sha & Bacchetti, 1997). Moreover, inhibition of telomerase results in death of tumor cells
615 *in vitro* and *in vivo* showing the importance of this enzyme for tumor growth (Hahn et al., 1999).
616 Similarly, various ERS responses have been shown to promote cell proliferation and survival in
617 various types of cancer (Zhang et al., 2024). These data suggest that *Acomys* can access and use
618 pathways other adult mammals do not outside of tumorigenesis.
619 As a functional test of cell type versus cell state as a driver of regeneration, we assessed
620 the role of CRABP1+ fibroblasts after injury in neonatal mice before this population disappears.
621 Previous studies have shown that papillary CRABP1+ fibroblasts are enriched in regenerative
622 neonatal human and mouse skin but are lost early during postnatal development (Mine et al.,
623 2008; Sinha et al., 2022). Examining neonatal and early postnatal stages, we found CRABP1+
624 fibroblasts in the *Mus* ear pinna which persisted until approximately P20. Using our ear punch
625 assay when CRABP1+ fibroblasts are present in the *Mus* ear pinna, did not improve ear hole
626 closure or stimulate regeneration. These results support that the presence of a cell population
627 alone may be less important that the ability for cells to acquire a specific cell state needed to
628 facilitate regeneration. A recent examination of regeneration and scarring phenotypes across
629 eleven murid rodents, underscored the binary nature of a regenerative phenotype in that species
630 appear to either completely regenerate or not (i.e., no partial regeneration) (Riddell et al., 2025).
631 This supports that complex tissue regeneration requires multiple features across stereotypical
632 healing processes such as intrinsic cell cycle licensing (Gawriluk et al., 2016; Tomasso et al.,
633 2023), goldilocks regulation of reactive oxygen species (ROS) (Saxena et al., 2019) and a
634 regenerative skewed immune cell response (Gawriluk et al., 2020; Simkin et al., 2017, 2024).
635 Future work investigating specific cell states across more regenerative and non-regenerative

636 mammals will undoubtably shed light on a blueprint for complex tissue regeneration in
637 mammals.
638

639 **ACKNOWLEDGEMENTS**

640 We would like to thank Josh Sarli, Brennan Riddell and Ava Musarra for animal husbandry. We
641 thank all members of the Seifert lab for helpful discussions in developing the manuscript and
642 Brennan Riddle for helping to create the GO graphs. This research was funded in part by grants
643 from the NIH (R01AR070313) and Aligning Science Across Parkinson's (ASAP-020495) through
644 the Michael J. Fox Foundation for Parkinson's Research (MJFF) to AWS. For the purpose of open
645 access, the author has applied a CC BY public copyright license to all Author Accepted
646 Manuscripts arising from this submission.
647

648 **AUTHOR CONTRIBUTIONS**

649 EOR, RA, and AWS designed research. EOR, MA and RA performed research. EOR, MA and
650 AWS analyzed data. EOR and AWS wrote the paper, and all authors commented on and edited the
651 paper.
652

653 **COMPETING INTERESTS**

654 The authors declare no competing interests.
655

656 **AVAILABILITY STATEMENT**

657 The data, code, protocols, and key lab materials used and generated in this study are listed in a
658 Key Resource Table alongside their persistent identifiers (Supplementary Tables).
659

660 **REFERENCES**

661

662 Audano, M., Pedretti, S., Cermenati, G., Brioschi, E., Diaferia, G. R., Ghisletti, S., Cuomo, A.,
663 Bonaldi, T., Salerno, F., Mora, M., Grigore, L., Garlaschelli, K., Baragetti, A., Bonacina, F.,
664 Catapano, A. L., Norata, G. D., Crestani, M., Caruso, D., Saez, E., … Mitro, N. (2018).
665 Zc3h10 is a novel mitochondrial regulator. *EMBO Reports*, *19*(4).
666 https://doi.org/10.15252/embr.201745531

667 Billingham, R. E., Mangold, R., & Silvers, W. K. (1959). THE NEOGENESIS OF SKIN IN THE
668 ANTLERS OF DEER*. *Annals of the New York Academy of Sciences*, *83*(3), 491–498.
669 https://doi.org/10.1111/J.1749-6632.1960.TB40922.X

670 Blanpain, C., & Fuchs, E. (2006). *Epidermal Stem Cells of the Skin*.

671 Borgens, R. B. (1982). Mice Regrow the Tips of Their Foretoes. *Science*, *217*(4561), 747–750.
672 https://doi.org/10.1126/SCIENCE.7100922

673 Brewer, C. M., Nelson, B. R., Wakenight, P., Collins, S. J., Okamura, D. M., Dong, X. R.,
674 Mahoney, W. M., McKenna, A., Shendure, J., Timms, A., Millen, K. J., & Majesky, M. W.
675 (2021). Adaptations in Hippo-Yap signaling and myofibroblast fate underlie scar-free ear
676 appendage wound healing in spiny mice. *Developmental Cell*, *56*(19), 2722–2740.
677 https://doi.org/10.1016/j.devcel.2021.09.008

678 Carlson, B. M. (2005). Some principles of regeneration in mammalian systems. *Anatomical*
679 *Record. Part B, New Anatomist*, *287*(1), 4–13. https://doi.org/10.1002/AR.B.20079

680 Chen, Y., Zhang, Z., Henson, E. S., Cuddihy, A., Haigh, K., Wang, R., Haigh, J. J., & Gibson, S.
681 B. (2022). Autophagy inhibition by TSSC4 (tumor suppressing subtransferable candidate 4)
682 contributes to sustainable cancer cell growth. *Autophagy*, *18*(6), 1274–1296.
683 https://doi.org/10.1080/15548627.2021.1973338

684 Cheung, T. H., & Rando, T. A. (2013). Molecular regulation of stem cell quiescence. In *Nature*
685 *Reviews Molecular Cell Biology* (Vol. 14, Issue 6, pp. 329–340).
686 https://doi.org/10.1038/nrm3591

687 Correa-Gallegos, D., Jiang, D., Christ, S., Ramesh, P., Ye, H., Wannemacher, J., Kalgudde Gopal,
688 S., Yu, Q., Aichler, M., Walch, A., Mirastschijski, U., Volz, T., & Rinkevich, Y. (2019).
689 Patch repair of deep wounds by mobilized fascia. *Nature*, *576*(7786), 287–292.
690 https://doi.org/10.1038/s41586-019-1794-y

691 Driskell, R. R., Lichtenberger, B. M., Hoste, E., Kretzschmar, K., Simons, B. D., Charalambous,
692 M., Ferron, S. R., Herault, Y., Pavlovic, G., Ferguson-Smith, A. C., & Watt, F. M. (2013).
693 Distinct fibroblast lineages determine dermal architecture in skin development and repair.
694 *Nature*, *504*(7479), 277–281. https://doi.org/10.1038/nature12783

695 Echeverri, K., Clarke, J. D. W., & Tanaka, E. M. (2001). In vivo imaging indicates muscle fiber
696 dedifferentiation is a major contributor to the regenerating tail blastema. *Developmental*
697 *Biology*, *236*(1), 151–164. https://doi.org/10.1006/dbio.2001.0312

698 Froehlich, J. M., Fowler, Z. G., Galt, N. J., Smith, D. L., & Biga, P. R. (2013). Sarcopenia and
699 piscines: The case for indeterminate-growing fish as unique genetic model organisms in aging
700 and longevity research. *Frontiers in Genetics*, *4*(AUG).
701 https://doi.org/10.3389/fgene.2013.00159

702 Gawriluk, T. R., Simkin, J., Hacker, C. K., Kimani, J. M., Kiama, S. G., Ezenwa, V. O., & Seifert,
703 A. W. (2020). Complex Tissue Regeneration in Mammals Is Associated With Reduced

Inflammatory Cytokines and an Influx of T Cells. *Frontiers in Immunology*, *11*. https://doi.org/10.3389/FIMMU.2020.01695/FULL

Gawriluk, T. R., Simkin, J., Thompson, K. L., Biswas, S. K., Clare-Salzler, Z., Kimani, J. M., Kiama, S. G., Smith, J. J., Ezenwa, V. O., & Seifert, A. W. (2016). Comparative analysis of ear-hole closure identifies epimorphic regeneration as a discrete trait in mammals. *Nature Communications*, *7*. https://doi.org/10.1038/ncomms11164

Gerber, T., Murawala, P., Knapp, D., Masselink, W., Schuez, M., Hermann, S., Gac-Santel, M., Nowoshilow, S., Kageyama, J., Khattak, S., Currie, J. D., Camp, J. G., Tanaka, E. M., & Treutlein, B. (2018). Single-cell analysis uncovers convergence of cell identities during axolotl limb regeneration. *Science*, *362*(6413). https://doi.org/10.1126/science.aaq0681

Goss, R. J. (1980). Prospects for Regeneration in Man. In *SECTION I11 BASIC SCIENCE AND PATHOLOGY*.

Goss, R. J., & Grimes, L. N. (1972). Tissue Interactions in the Regeneration of Rabbit Ear Holes. In *AM. Zooi.or.isr* (Vol. 12). https://academic.oup.com/icb/article/12/1/151/2107413

Gu, W., Schneider, J. W., Condorelli, G., Kaushai, S., Yahdavi, V., & Nadai-Ginard, B. (1993). Intmion of Myogenic Factors and the l%tinobl ma Protein Muscle Cell Commitment and Dmeren#ation. In *Cell* (Vol. 72).

Guerrero-Juarez, C. F., Dedhia, P. H., Jin, S., Ruiz-Vega, R., Ma, D., Liu, Y., Yamaga, K., Shestova, O., Gay, D. L., Yang, Z., Kessenbrock, K., Nie, Q., Pear, W. S., Cotsarelis, G., & Plikus, M. V. (2019). Single-cell analysis reveals fibroblast heterogeneity and myeloid-derived adipocyte progenitors in murine skin wounds. *Nature Communications*, *10*(1). https://doi.org/10.1038/s41467-018-08247-x

HAHN, W. C., STEWART, S. A., BROOKS, M. W., YORK, S. G., EATON, E., KURACHI, A., BEIJERSBERGEN, R. L., KNOLL, J. H. M., MEYERSON, M., & WEINBERG, R. A. (1999). Inhibition of telomerase limits the growth of human cancer cells. *Nature*.

Hanahan, D., & Weinberg, R. A. (2011). Hallmarks of cancer: The next generation. In *Cell* (Vol. 144, Issue 5, pp. 646–674). https://doi.org/10.1016/j.cell.2011.02.013

Hao, Y., Stuart, T., Kowalski, M. H., Choudhary, S., Hoffman, P., Hartman, A., Srivastava, A., Molla, G., Madad, S., Fernandez-Granda, C., & Satija, R. (2024). Dictionary learning for integrative, multimodal and scalable single-cell analysis. *Nature Biotechnology*, *42*(2), 293–304. https://doi.org/10.1038/s41587-023-01767-y

Hays, E. D., & Fischman, D. A. (1961). Origin of the Blastema in Regenerating Limbs of the Newt Triturus viridescens An Autoradiographic Study Using Tritiated Thymidine to Follow Cell Proliferation and MFgration'. In *DEVELOPMENTAL BIOLOGY* (Vol. 3).

Jiang, D., & Rinkevich, Y. (2021). Distinct fibroblasts in scars and regeneration. In *Current Opinion in Genetics and Development* (Vol. 70, pp. 7–14). Elsevier Ltd. https://doi.org/10.1016/j.gde.2021.04.005

Johnson, G. L., Masias, E. J., & Lehoczky, J. A. (2020). Cellular Heterogeneity and Lineage Restriction during Mouse Digit Tip Regeneration at Single-Cell Resolution. *Developmental Cell*, *52*(4), 525-540.e5. https://doi.org/10.1016/j.devcel.2020.01.026

Johnson, K., Bateman, J., DiTommaso, T., Wong, A. Y., & Whited, J. L. (2018). Systemic cell cycle activation is induced following complex tissue injury in axolotl. *Developmental Biology*, *433*(2), 461–472. https://doi.org/10.1016/j.ydbio.2017.07.010

Jopling, C., Sleep, E., Raya, M., Martí, M., Raya, A., & Belmonte, J. C. I. (2010). Zebrafish heart regeneration occurs by cardiomyocyte dedifferentiation and proliferation. *Nature*, *464*(7288), 606–609. https://doi.org/10.1038/nature08899

Joseph, J., & Dyson, M. (1966). Tissue replacement in the rabbit's ear. *The British Journal of Surgery*, *53*(4), 372–380. https://doi.org/10.1002/BJS.1800530415

Kim, Nam. W., Piatyszek, Miezyslaw. A., Prowse, Karen. R., Harley, Calvin. B., West, Michael. D., Ho, Peter. L. C., Coviello, Gina. M., Wright, Woodring. E., Weinrich, Scott. L., & Shay, Jerry. W. (1994). Specific association of human telomerase activity with immortal cells and cancer. *Science*.

Lehoczky, J. A., Robert, B., & Tabin, C. J. (2011). Mouse digit tip regeneration is mediated by fate-restricted progenitor cells. *Proceedings of the National Academy of Sciences of the United States of America*, *108*(51), 20609–20614. https://doi.org/10.1073/pnas.1118017108

Leigh, N. D., Dunlap, G. S., Johnson, K., Mariano, R., Oshiro, R., Wong, A. Y., Bryant, D. M., Miller, B. M., Ratner, A., Chen, A., Ye, W. W., Haas, B. J., & Whited, J. L. (2018). Transcriptomic landscape of the blastema niche in regenerating adult axolotl limbs at single-cell resolution. *Nature Communications*, *9*(1). https://doi.org/10.1038/s41467-018-07604-0

Liu, L., Michowski, W., Kolodziejczyk, A., & Sicinski, P. (2019). The cell cycle in stem cell proliferation, pluripotency and differentiation. In *Nature Cell Biology* (Vol. 21, Issue 9, pp. 1060–1067). Nature Publishing Group. https://doi.org/10.1038/s41556-019-0384-4

Maden, M., & Wallace, H. (1976). *How X-Rays inhibit Amphibian Limb Regeneration*.

Mine, S., Fortunel, N. O., Pageon, H., & Asselineau, D. (2008). Aging alters functionally human dermal papillary fibroblasts but not reticular fibroblasts: A new view of skin morphogenesis and aging. *PLoS ONE*, *3*(12). https://doi.org/10.1371/journal.pone.0004066

Morgan, T. H. (1901). *Regeneration /*. New York : http://hdl.handle.net/2027/mdp.39015001913774

Nechiporuk, A., & Keating, M. T. (2002). A proliferation gradient between proximal and msxb-expressing distal blastema directs zebrafish fin regeneration. *Development*.

Neeham, A. (1953). Regeneration and Wound-healing. *BioScience*, *3*(1), 16–16. https://doi.org/10.1093/AIBSBULLETIN/3.1.16-F

Orford, K. W., & Scadden, D. T. (2008). Deconstructing stem cell self-renewal: Genetic insights into cell-cycle regulation. In *Nature Reviews Genetics* (Vol. 9, Issue 2, pp. 115–128). https://doi.org/10.1038/nrg2269

Pajcini, K. V., Corbel, S. Y., Sage, J., Pomerantz, J. H., & Blau, H. M. (2010). Transient inactivation of Rb and ARF yields regenerative cells from postmitotic mammalian muscle. *Cell Stem Cell*, *7*(2), 198–213. https://doi.org/10.1016/j.stem.2010.05.022

Phan, Q. M., Sinha, S., Biernaskie, J., & Driskell, R. R. (2021a). Single-cell transcriptomic analysis of small and large wounds reveals the distinct spatial organization of regenerative fibroblasts. *Experimental Dermatology*, *30*(1), 92–101. https://doi.org/10.1111/exd.14244

Phan, Q. M., Sinha, S., Biernaskie, J., & Driskell, R. R. (2021b). Single-cell transcriptomic analysis of small and large wounds reveals the distinct spatial organization of regenerative fibroblasts. *Experimental Dermatology*, *30*(1), 92–101. https://doi.org/10.1111/exd.14244

Plikus, M. V, Guerrero-Juarez, C. F., Ito, M., Li, Y. R., Dedhia, P. H., Zheng, Y., Shao, M., Gay, D. L., Ramos, R., Hsi, T.-C., Oh, J. W., Wang, X., Ramirez, A., Konopelski, S. E., Elzein, A., Wang, A., Supapannachart, R. J., Lee, H.-L., Lim, C. H., … Cotsarelis, G. (2017). *Regeneration of fat cells from myofibroblasts during wound healing*. https://www.science.org

Plikus, M. V., Wang, X., Sinha, S., Forte, E., Thompson, S. M., Herzog, E. L., Driskell, R. R., Rosenthal, N., Biernaskie, J., & Horsley, V. (2021). Fibroblasts: Origins, definitions, and functions in health and disease. In *Cell* (Vol. 184, Issue 15, pp. 3852–3872). Elsevier B.V. https://doi.org/10.1016/j.cell.2021.06.024

Poleo, G., Brown, C. W., Laforest, L., & Akimenko, M. A. (2001). Cell proliferation and movement during early fin regeneration in zebrafish. In *Developmental Dynamics* (Vol. 221, Issue 4, pp. 380–390). https://doi.org/10.1002/dvdy.1152

Riddell, B., McDonough, M., Ferguson, A., Kimani, J. M., Gawriluk, T. R., Peng, C., Kiama, S. G., Ezenwa, V. O., & Seifert, A. W. (2025). Complex tissue regeneration in Lophuromys reveals a phylogenetic signal for enhanced regenerative ability in deomyine rodents. *Proceedings of the National Academy of Sciences of the United States of America*, *122*(1). https://doi.org/10.1073/PNAS.2420726122

Rinkevich, Y., Lindau, P., Ueno, H., Longaker, M. T., & Weissman, I. L. (2011). Germ-layer and lineage-restricted stem/progenitors regenerate the mouse digit tip. *Nature*, *476*(7361), 409–414. https://doi.org/10.1038/nature10346

Rodgers, J. T., King, K. Y., Brett, J. O., Cromie, M. J., Charville, G. W., Maguire, K. K., Brunson, C., Mastey, N., Liu, L., Tsai, C. R., Goodell, M. A., & Rando, T. A. (2014). MTORC1 controls the adaptive transition of quiescent stem cells from G 0 to GAlert. *Nature*, *510*(7505), 393–396. https://doi.org/10.1038/nature13255

Saxena, S., Vekaria, H., Sullivan, P. G., & Seifert, A. W. (2019). Connective tissue fibroblasts from highly regenerative mammals are refractory to ROS-induced cellular senescence. *Nature Communications*, *10*(1). https://doi.org/10.1038/s41467-019-12398-w

Schneider, J. W., Gu, W., Zhu, L., Mahdavi, V., & Nadal-Ginard, B. (1994). Reversal of Terminal Differentiation Mediated by p107 in Rb-/- Muscle Cells. In *New Series* (Vol. 264, Issue 5164).

Sebens, K. P. (1987). The ecology of indeterminate growth in animals. *Ann. Rev. Ecol. Syst*.

Seifert, A. W., Kiama, S. G., Seifert, M. G., Goheen, J. R., Palmer, T. M., & Maden, M. (2012). Skin shedding and tissue regeneration in African spiny mice (Acomys). *Nature*, *489*(7417), 561–565. https://doi.org/10.1038/nature11499

Seifert, A. W., & Muneoka, K. (2018). The blastema and epimorphic regeneration in mammals. In *Developmental Biology* (Vol. 433, Issue 2, pp. 190–199). Elsevier Inc. https://doi.org/10.1016/j.ydbio.2017.08.007

Sha, J. W., & Bacchetti, S. (1997). A Survey of Telomerase Activity in Human Cancer. In *Eur J Cancer* (Vol. 33, Issue 5).

Simkin, J., Aloysius, A., Adam, M., Safaee, F., Donahue, R. R., Biswas, S., Lakhani, Z., Gensel, J. C., Thybert, D., Potter, S., & Seifert, A. W. (2024). Tissue-resident macrophages specifically express Lactotransferrin and Vegfc during ear pinna regeneration in spiny mice. *Developmental Cell*, *59*(4), 496-516.e6. https://doi.org/10.1016/j.devcel.2023.12.017

Simkin, J., Gawriluk, T. R., Gensel, J. C., & Seifert, A. W. (2017). *Macrophages are necessary for epimorphic regeneration in African spiny mice*. https://doi.org/10.7554/eLife.24623.001

Simkin, J., & Seifert, A. W. (2018). Concise Review: Translating Regenerative Biology into Clinically Relevant Therapies: Are We on the Right Path? In *Stem Cells Translational Medicine* (Vol. 7, Issue 2, pp. 220–231). John Wiley and Sons Ltd. https://doi.org/10.1002/sctm.17-0213

Sinha, S., Sparks, H. D., Labit, E., Robbins, H. N., Gowing, K., Jaffer, A., Kutluberk, E., Arora, R., Raredon, M. S. B., Cao, L., Swanson, S., Jiang, P., Hee, O., Pope, H., Workentine, M., Todkar, K., Sharma, N., Bharadia, S., Chockalingam, K., … Biernaskie, J. (2022). Fibroblast inflammatory priming determines regenerative versus fibrotic skin repair in reindeer. *Cell*, *185*(25), 4717-4736.e25. https://doi.org/10.1016/j.cell.2022.11.004

Storer, M. A., Mahmud, N., Karamboulas, K., Borrett, M. J., Yuzwa, S. A., Gont, A., Androschuk, A., Sefton, M. V., Kaplan, D. R., & Miller, F. D. (2020). Acquisition of a Unique Mesenchymal Precursor-like Blastema State Underlies Successful Adult Mammalian Digit Tip Regeneration. *Developmental Cell*, *52*(4), 509-524.e9. https://doi.org/10.1016/j.devcel.2019.12.004

Tanaka, E. M., & Brockes, J. P. (1998). A target of thrombin activation promotes cell cycle re-entry by urodele muscle cells. *Wound Repair and Regeneration*, *6*(4), S-371-S-381. https://doi.org/10.1046/J.1524-475X.1998.60413.X/FORMAT/PDF

Tanaka, E. M., Gann, A. A. F., Gates, P. B., & Brockes, J. P. (1997). Newt Myotubes Reenter the Cell Cycle by Phosphorylation of the Retinoblastoma Protein. In *The Journal of Cell Biology* (Vol. 136, Issue 1).

Tomasso, A., Koopmans, T., Lijnzaad, P., Bartscherer, K., & Seifert, A. W. (2023). *An ERK-dependent molecular switch antagonizes fibrosis and promotes regeneration in spiny mice (Acomys)*. https://www.science.org

Vorontsova, M. A., Liosner, L. D., Allen, P. M., & Billett, F. (1960). *Asexual propagation and regeneration*.

Wallace, H. (1981). *Vertebrate Limb Regeneration* (John Wiley & Sons, Ed.; First edition).

Wallace, H., & Maden, M. (1976). THE CELL CYCLE DURING AMPHIBIAN LIMB REGENERATION. In *J. CeUSci.zo*.

Wenemoser, D., & Reddien, P. W. (2010). Planarian regeneration involves distinct stem cell responses to wounds and tissue absence. *Developmental Biology*, *344*(2), 979–991. https://doi.org/10.1016/j.ydbio.2010.06.017

Zhang, W., Shi, Y., Oyang, L., Cui, S., Li, S., Li, J., Liu, L., Li, Y., Peng, M., Tan, S., Xia, L., Lin, J., Xu, X., Wu, N., Peng, Q., Tang, Y., Luo, X., Liao, Q., Jiang, X., & Zhou, Y. (2024). Endoplasmic reticulum stress—a key guardian in cancer. In *Cell Death Discovery* (Vol. 10, Issue 1). Springer Nature. https://doi.org/10.1038/s41420-024-02110-3

FIGURES AND LEGENDS

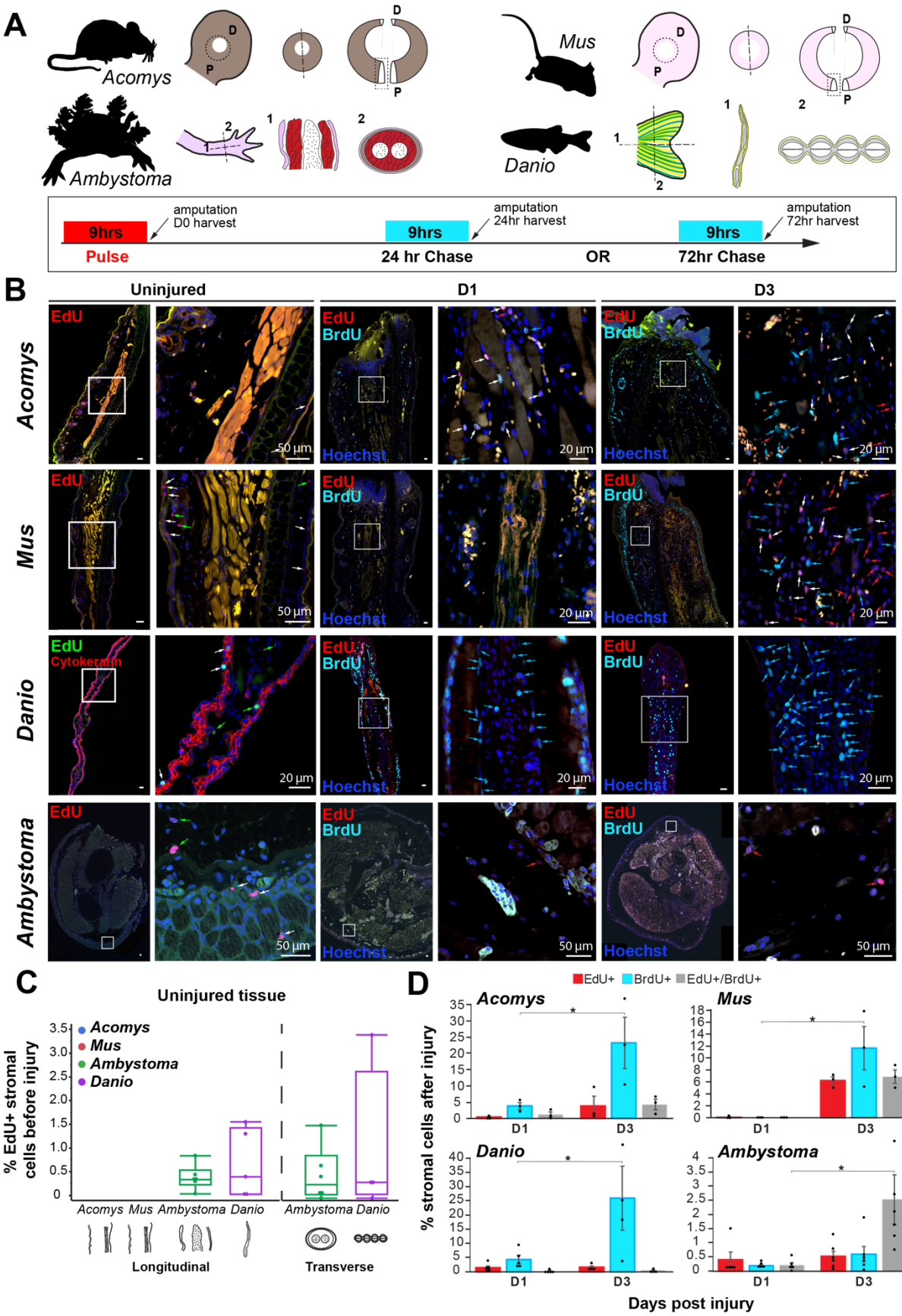
A
Acomys
Mus
Ambystoma
Danio
9hrs
amputation D0 harvest
Pulse
9hrs
amputation 24hr harvest
24 hr Chase
OR
9hrs
amputation 72hr harvest
72hr Chase
B
Uninjured
D1
D3
Acomys
Mus
Danio
Ambystoma
EdU
BrdU
Hoechst
Cytokeratin
50 µm
20 µm
C
Uninjured tissue
% EdU+ stromal cells before injury
Acomys
Mus
Ambystoma
Danio
Longitudinal
Transverse
D
EdU+
BrdU+
EdU+/BrdU+
% stromal cells after injury
Days post injury
D1
D3

883

884 **Figure 1. Cell cycle re-entry before and after injury in *Acomys*, *Mus*, *Danio* and**
885 ***Ambystoma*.** A) Tissue section planes and EdU/BrdU pulse-chase scheme indicating injections
886 and harvest times; D = distal, P = proximal. B) Representative images of EdU+ and BrdU+ cells
887 in uninjured tissue (D0), D1 and D3. In uninjured tissue, white arrows = positive cells in the
888 epidermis and green arrows = positive cells in the stromal compartment. In injured tissue, red
889 arrows = EdU+ cells, light blue arrows = BrdU+ cells, and white arrows = double positive cells
890 (EdU+/BrdU+). C) EdU+ cell quantification as a percentage of the total number of cells in
891 uninjured tissue from all four species. Autofluorescent tissue, including red blood cells, stains in
892 multiple channels (yellow). D) EdU+, Brdu+ and EdU+/BrdU+ cell quantification as a
893 percentage of the total number of cells at D1 and D3 post-injury. Images represent n = 3
894 biological samples/time point in *Acomys* and *Mus*. See Methods for cell counting quantification.
895 In *Danio* (zebrafish), n = 9 at D0, n = 5 at D1 and n = 4 at D3. In *Ambystoma* (axolotl), n = 12 at
896 D0, n = 6 at D1, n = 6 at D3. (* $p<0.05$, ** $p<0.01$).

897

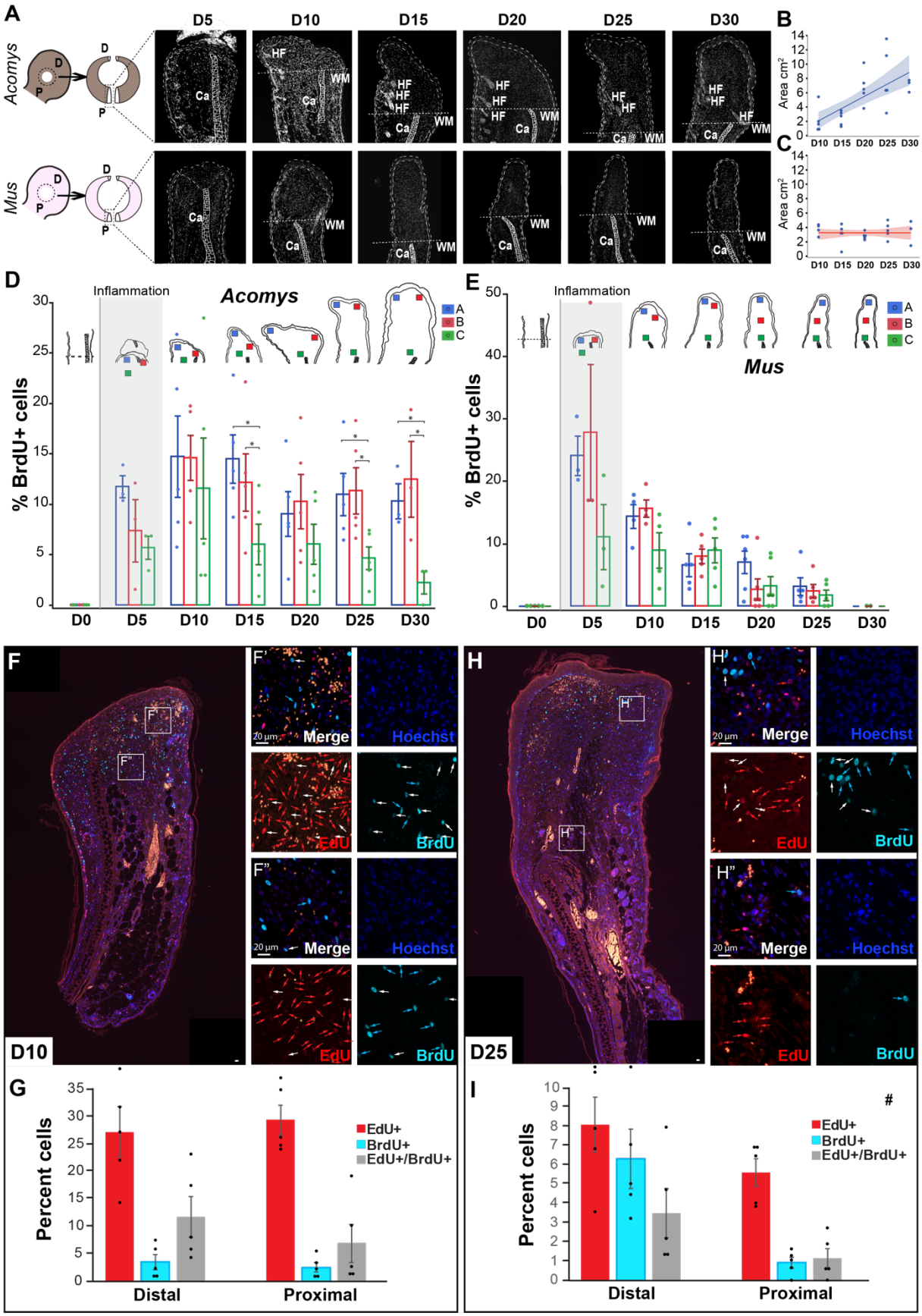
A
Acomys
Mus
D5
D10
D15
D20
D25
D30
Ca
HF
WM
B
C
Area cm²
D10 D15 D20 D25 D30
D
E
Inflammation
Acomys
Mus
% BrdU+ cells
A
B
C
D0 D5 D10 D15 D20 D25 D30
F
F'
F"
H
H'
H"
Merge
Hoechst
EdU
BrdU
20 µm
D10
D25
G
I
Percent cells
EdU+
BrdU+
EdU+/BrdU+
Distal
Proximal
#

898

899 **Figure 2. Spatiotemporal distribution of proliferating cells in *Acomys* and *Mus*.** A)
900 Representative images of blastema and scar tissue changes over time (D5-D30), Ca = cartilage,
901 WM = wound margin, HF = hair follicle. B-C) Blastema or scar tissue area in mm^2 from D10 to
902 D30 based on tissue sections. D-E) Quantification of BrdU+ cells as a percentage of the total
903 number of cells in three areas (A = blue, B = red, C = green) of the blastema in *Acomys* or the
904 scar in *Mus* from D5 to D30. F-H) Representative images of D10 (F) and D25 (H) blastema
905 tissue with EdU+, BrdU+ and double positive cells. Red arrows = EdU+ cells, light blue arrows
906 = BrdU+ cells, and white arrows = double positive cells (EdU+/BrdU+). G-I) Quantification of
907 EdU+, BrdU+ and EdU+/BrdU+ cells as a percentage of the total number of cells in distal and
908 proximal areas relative to the wound site at D10 (G) and D25 (I). n = 5 per time point per
909 species. (* $p<0.05$).

910

911

912

913

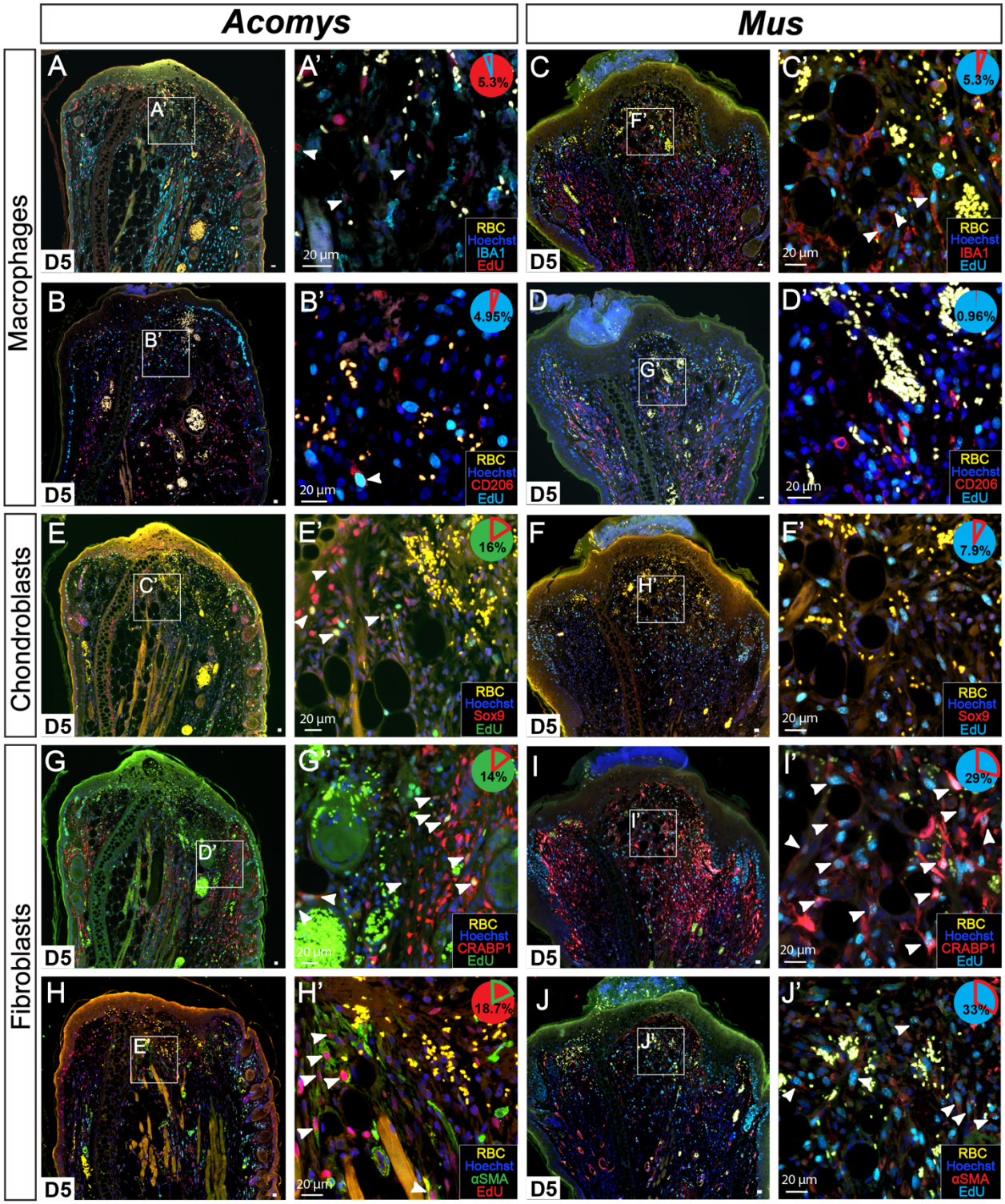

Figure 3. S-phase quantification of fibroblasts, chondroblasts and macrophages after injury at D5 in *Acomys* and *Mus*. A-D) Cycling macrophages double labeled with IBA1 and EdU in *Acomys* (A-A') and *Mus* (C-C') or with CD206 and EdU in *Acomys* (B-B') and *Mus* (D-

918 D'). E-F) Chondroblasts double labeled with Sox9 and EdU in *Acomys* (E-E') and *Mus* (F-F').
919 G-J) Fibroblasts double labeled with CRABP1 and EdU in *Acomys* (G-G') and *Mus* (I-I'). or
920 with αSMA and EdU in *Acomys* (H-H') and *Mus* (J-J'). White arrows indicate double positive
921 cells (EdU+/cell type marker). Pie charts indicate percentage double positive cells of the total
922 number of counted EdU+ cells. n = 5/species. RBC = red blood cells.

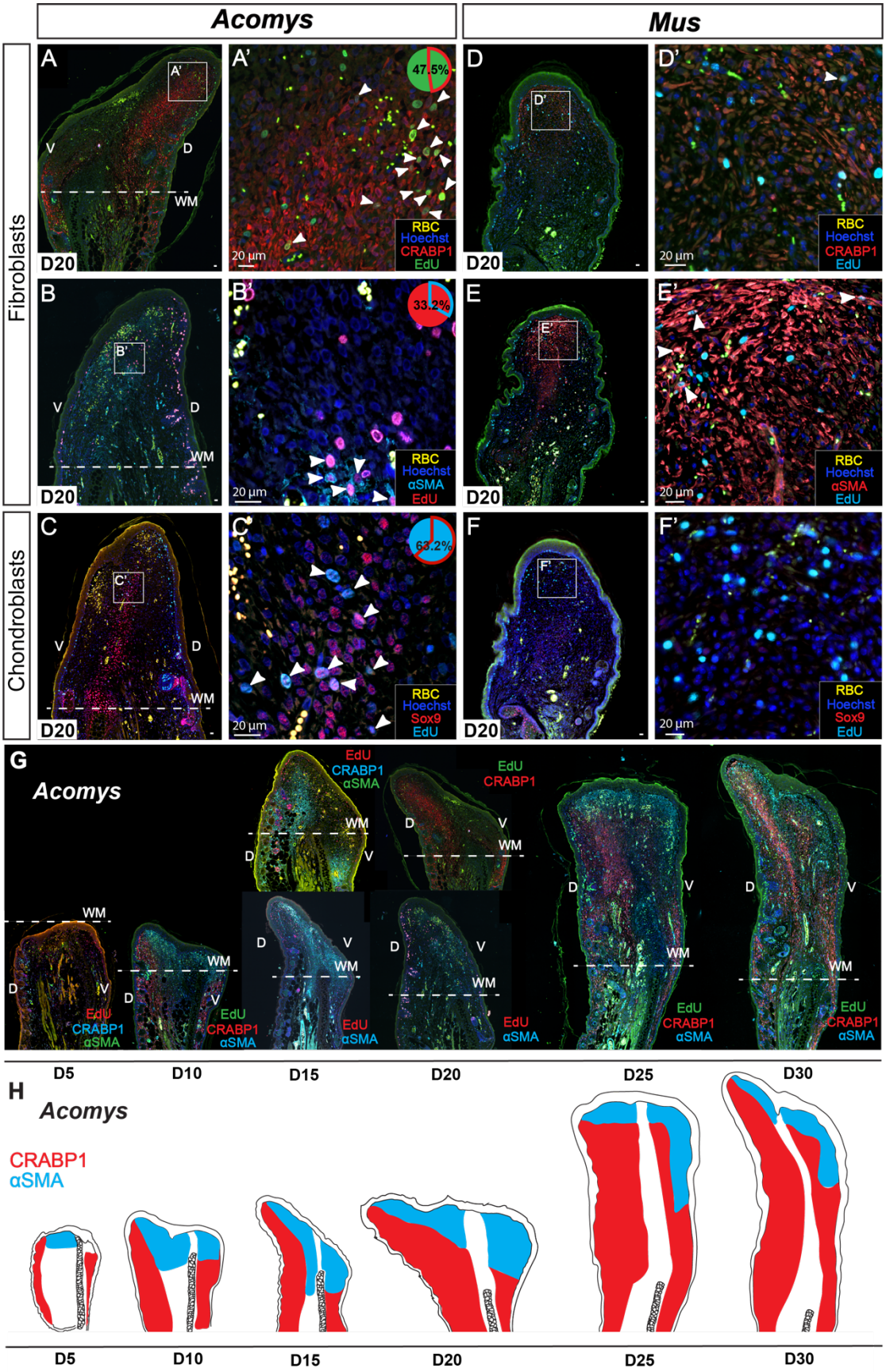
Acomys
Mus
Fibroblasts
Chondroblasts
A
A'
B
B'
C
C'
D
D'
E
E'
F
F'
V
D
WM
D20
47.5%
33.2%
63.2%
20 µm
RBC
Hoechst
CRABP1
αSMA
Sox9
EdU
G
Acomys
EdU
CRABP1
αSMA
H
Acomys
CRABP1
αSMA
D5
D10
D15
D20
D25
D30

924 **Figure 4. Spatial distribution of cell types within blastema or scar at D20.** A-C) CRABP1+
925 (A-A') or αSMA+ (B-B') fibroblasts, and Sox9+ chondroblasts (C-C') in *Acomys* at D20. D-F)
926 CRABP1+ (D-D') or αSMA+ (E-E') fibroblasts, and Sox9+ chondroblasts (F-F') in *Mus* at D20.
927 G) CRABP1 and αSMA double staining in *Acomys* over time (D5-D30). H) Cartoon showing
928 general distribution of CRABP1+ and αSMA+ fibroblasts in *Acomys.* White arrows indicate
929 double positive cells (EdU+/cell type marker). Pie charts indicate percentage double positive of
930 the total number of counted EdU+ cells. n = 5 per species. RBC = red blood cells.

931

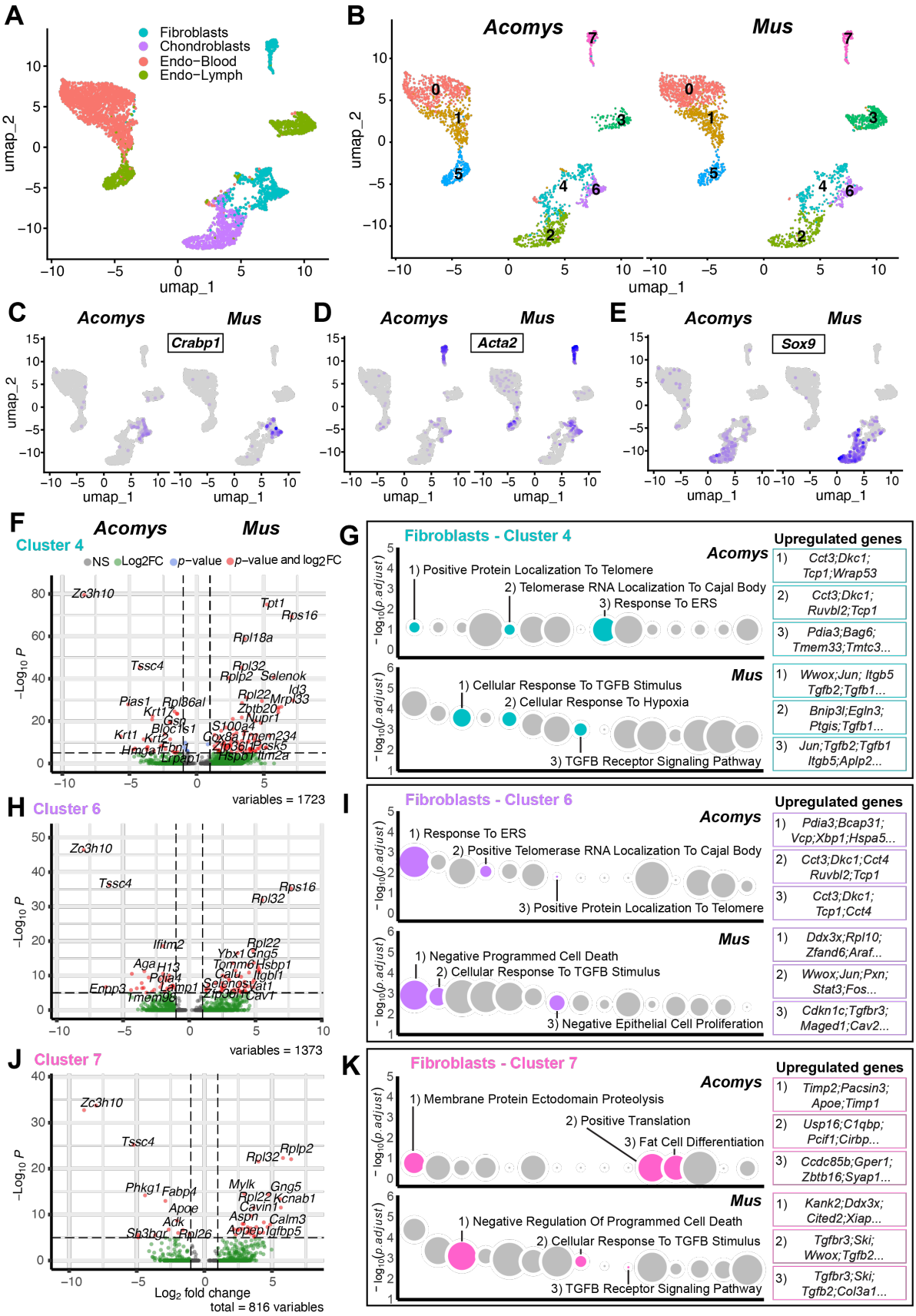
A
Fibroblasts
Chondroblasts
Endo−Blood
Endo−Lymph
umap_1
umap_2
B
Acomys
Mus
C
Crabp1
D
Acta2
E
Sox9
F
Cluster 4
NS Log2FC p−value p−value and log2FC
variables = 1723
H
Cluster 6
variables = 1373
J
Cluster 7
Log2 fold change
total = 816 variables
G
Fibroblasts - Cluster 4
1) Positive Protein Localization To Telomere
2) Telomerase RNA Localization To Cajal Body
3) Response To ERS
1) Cellular Response To TGFB Stimulus
2) Cellular Response To Hypoxia
3) TGFB Receptor Signaling Pathway
Upregulated genes
1) Cct3;Dkc1; Tcp1;Wrap53
2) Cct3;Dkc1; Ruvbl2;Tcp1
3) Pdia3;Bag6; Tmem33;Tmtc3...
1) Wwox;Jun; Itgb5 Tgfb2;Tgfb1...
2) Bnip3l;Egln3; Ptgis;Tgfb1...
3) Jun;Tgfb2;Tgfb1 Itgb5;Aplp2...
I
Fibroblasts - Cluster 6
1) Response To ERS
2) Positive Telomerase RNA Localization To Cajal Body
3) Positive Protein Localization To Telomere
1) Negative Programmed Cell Death
2) Cellular Response To TGFB Stimulus
3) Negative Epithelial Cell Proliferation
1) Pdia3;Bcap31; Vcp;Xbp1;Hspa5...
2) Cct3;Dkc1;Cct4 Ruvbl2;Tcp1
3) Cct3;Dkc1; Tcp1;Cct4
1) Ddx3x;Rpl10; Zfand6;Araf...
2) Wwox;Jun;Pxn; Stat3;Fos...
3) Cdkn1c;Tgfbr3; Maged1;Cav2...
K
Fibroblasts - Cluster 7
1) Membrane Protein Ectodomain Proteolysis
2) Positive Translation
3) Fat Cell Differentiation
1) Negative Regulation Of Programmed Cell Death
2) Cellular Response To TGFB Stimulus
3) TGFB Receptor Signaling Pathway
1) Timp2;Pacsin3; Apoe;Timp1
2) Usp16;C1qbp; Pcif1;Cirbp...
3) Ccdc85b;Gper1; Zbtb16;Syap1...
1) Kank2;Ddx3x; Cited2;Xiap...
2) Tgfbr3;Ski; Wwox;Tgfb2...
3) Tgfbr3;Ski; Tgfb2;Col3a1...

932

933 **Figure 5. Single-cell analysis reveals different fibroblast cell states in *Acomys* and *Mus*.** Cell
934 suspensions collected from healing tissue preps representing D0, 3, 5, 10 and 15 were batch-
935 corrected and plotted together (Fig. S7) (see Methods). A) UMAP projection of stromal cell
936 types re-clustered from all cells (Fig. S7) from both species. B) UMAP projection of stromal
937 subpopulations separated by species. Clusters represent subpopulations of major subtypes
938 indicated in A. C-E) Feature plots for *Crabp1* (C), *Acta2* (D), and *Sox9* (E) separated by species.
939 F, H, J) Volcano plots showing differentially upregulated genes between *Acomys* and *Mus* from
940 clusters four (F), six (H), and seven (J) in B. Gene ontology Biological Process based on
941 differentially upregulated genes between *Acomys* and *Mus* clusters four (G), six (I), and seven
942 (K). Dot size represents the relative number of genes in each plot. Upregulated genes associated
943 with each pathway are in color boxes. Refer to supplementary table S4 to see full list of genes.

944

945

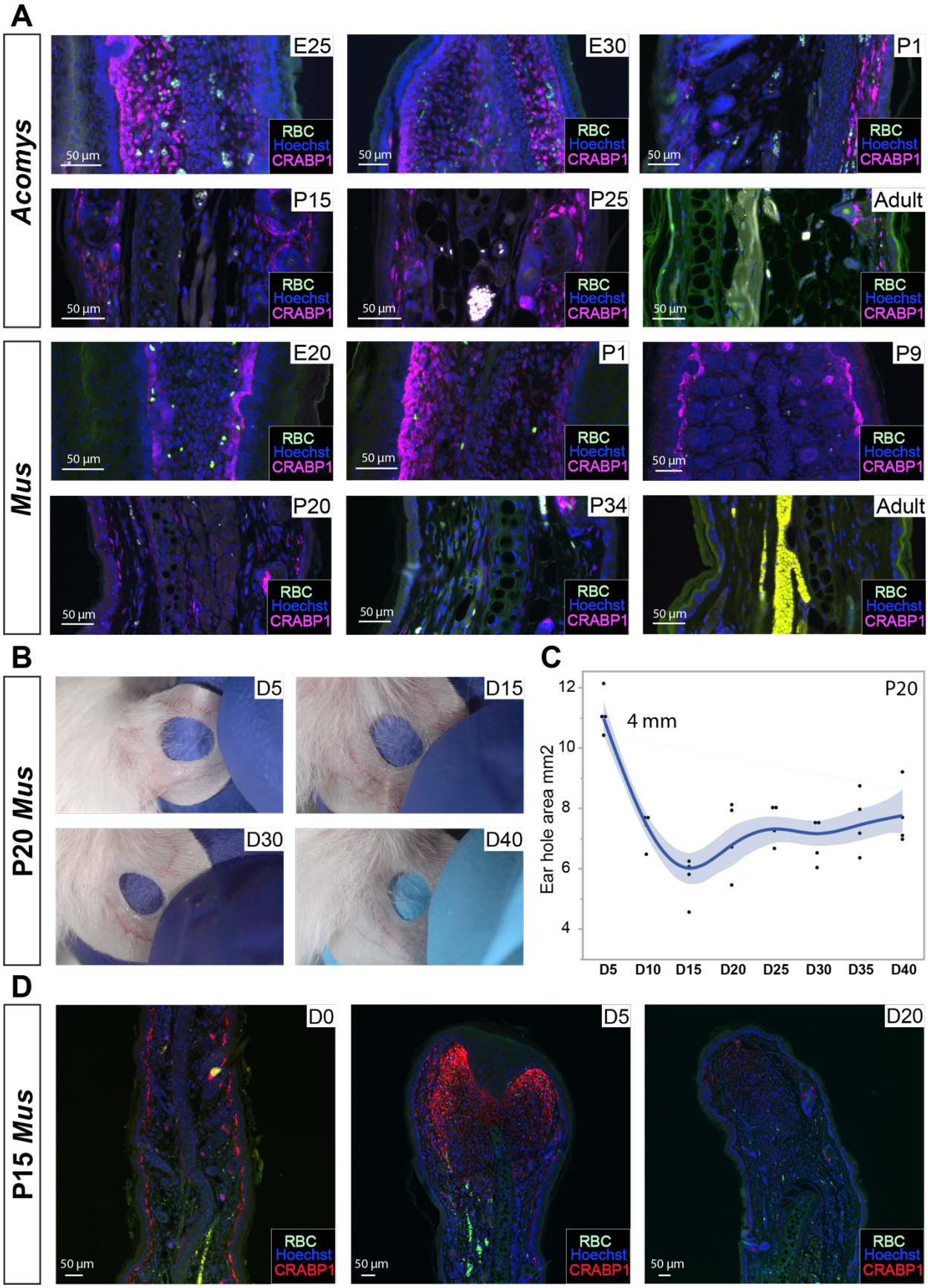
A
Acomys
E25
E30
P1
P15
P25
Adult
Mus
E20
P1
P9
P20
P34
Adult
RBC
Hoechst
CRABP1
50 µm
B
P20 Mus
D5
D15
D30
D40
C
P20
4 mm
Ear hole area mm2
12
10
8
6
4
D5
D10
D15
D20
D25
D30
D35
D40
D
P15 Mus
D0
D5
D20

946

947 **Figure 6. Tissue injury in neonatal mouse ears when CRABP1+ fibroblasts are present**
948 **does not facilitate regeneration.** A) Immunostaining for CRABP1 in *Acomys* and *Mus*. Age in
949 days indicated in upper right corner of each image. B) Images showing representative ear hole
950 closure from P20 injured *Mus* after a 4 mm ear punch. C) Quantification of ear hole closure area
951 from D5 to D40. D) CRABP1 staining in P15 *Mus* before and after injury. n = 3 per species per
952 time point. Green channel shows autofluorescence including red blood cells (RBC).

953

954